JGR Space Physics

REVIEW ARTICLE
10.1029/2021JA029538

Special Section:
Cluster 20th Anniversary: Results from the First 3D Mission

Curlometer Technique and Applications

M. W. Dunlop[1,2,3], X.-C. Dong[2], T.-Y. Wang[2], J. P. Eastwood[3], P. Robert[4], S. Haaland[5,6,7], Y.-Y. Yang[8], P. Escoubet[9], Z.-J. Rong[10], C. Shen[11], H.-S. Fu[1], and J. De Keyser[12]

[1]School of Space and Environment, Beihang University, Beijing, China, [2]RAL, Oxfordshire, UK, [3]Space and Atmospheric physics, Imperial College London, London, UK, [4]Laboratoire de Physique des Plasmas, Ecole Polytechnique, Palaiseau, France, [5]Birkeland Centre for Space Science, University of Bergen, Bergen, Norway, [6]The University Centre in Svalbard, Longyearbyen, Svalbard, [7]Max-Planck Institute for Solar Systems Research, Goettingen, Germany, [8]Geophyscics & Space Physics of ICD, CEA, Beijing, China, [9]ESA/ESTEC, AG Noordwijk, The Netherlands, [10]Institute of Geology and Geophysics, Chinese Academy of Sciences, Beijing, China, [11]Harbin Institute of Technology, Shenzhen, China, [12]Royal Belgian Institute for Space Aeronomy, Brussels, Belgium

Abstract We review the range of applications and use of the curlometer, initially developed to analyze Cluster multi-spacecraft magnetic field data; but more recently adapted to other arrays of spacecraft flying in formation, such as MMS small-scale, 4-spacecraft configurations; THEMIS close constellations of 3–5 spacecraft, and Swarm 2–3 spacecraft configurations. Although magnetic gradients require knowledge of spacecraft separations and the magnetic field, the structure of the electric current density (for example, its relative spatial scale), and any temporal evolution, limits measurement accuracy. Nevertheless, in many magnetospheric regions the curlometer is reliable (within certain limits), particularly under conditions of time stationarity, or with supporting information on morphology (for example, when the geometry of the large scale structure is expected). A number of large-scale regions have been covered, such as: the cross-tail current sheet, ring current, the current layer at the magnetopause and field-aligned currents. Transient and smaller scale current structures (e.g., reconnected flux tube or dipolarisation fronts) and energy transfer processes. The method is able to provide estimates of single components of the vector current density, even if there are only two or three satellites flying in formation, within the current region, as can be the case when there is a highly irregular spacecraft configuration. The computation of magnetic field gradients and topology in general includes magnetic rotation analysis and various least squares approaches, as well as the curlometer, and indeed the added inclusion of plasma measurements and the extension to larger arrays of spacecraft have recently been considered.

Plain Language Summary This article is an account of the curlometer method which was designed to estimate the electric current density from measurements of the magnetic field taken on board the four Cluster II spacecraft. It has been used very extensively in many regions of the magnetosphere, and has been applied to data from other spacecraft. The technique is robust and is known to be stable under certain conditions. It has also been integrated into other techniques dealing with the geometry of the magnetic field and its gradients in space.

Key Points:

- Robust multi-spacecraft analysis method using the magnetic field
- Allows the estimate of the vector electric current density directly
- Has been applied widely in many regions of the magnetosphere

Correspondence to:
M. W. Dunlop,
m.w.dunlop@rl.ac.uk

Citation:
Dunlop, M. W., Dong, X.-C., Wang, T.-Y., Eastwood, J. P., Robert, P., Haaland, S., et al. (2021). Curlometer technique and applications. *Journal of Geophysical Research: Space Physics*, *126*, e2021JA029538. https://doi.org/10.1029/2021JA029538

Received 5 MAY 2021
Accepted 25 OCT 2021

Author Contributions:
Conceptualization: M. W. Dunlop, S. Haaland
Formal analysis: X.-C. Dong
Methodology: M. W. Dunlop, J. P. Eastwood, P. Robert, Y.-Y. Yang, Z.-J. Rong, C. Shen, J. De Keyser
Writing – original draft: M. W. Dunlop, X.-C. Dong
Writing – review & editing: X.-C. Dong, T.-Y. Wang, J. P. Eastwood, P. Robert, S. Haaland, Y.-Y. Yang, P. Escoubet, Z.-J. Rong, C. Shen, H.-S. Fu, J. De Keyser

1. Introduction

The successful launches of the four Cluster II spacecraft (Escoubet et al., 2001), which began full science operations in eccentric polar orbits in February 2001, heralded a step change in the exploration and analysis of the Earth's magnetosphere, magnetosheath and near-Earth upstream (solar wind) regions. For the first time 3-D structure and temporal evolution could be probed and partly separated through an evolving spatial array, which allows spatial gradients (in particular) of key quantities to be analyzed. Such analysis was in fact long anticipated with a number of early designs of methods specifically for Cluster data: an ISSI working team producing the first book on collected multi-spacecraft analysis techniques in 1998 (Paschmann & Daly, 1998). The left hand side of Figure 1 shows that on the dayside the orbit began as a polar, asymmetric, inertial orbit ($4 \times 19.6\ R_E$), but later fuel conservation and correction manoeuvres resulted in a modified orbit with the inclination rolling over and a changing apogee height and position. Cluster maintained a phased configuration for much of its operating life and remains the only space physics mission to do this with fully four-point coverage on such a large range of spatial scales, spanning two solar cycles. The right hand side of Figure 1 shows the spacecraft separation for

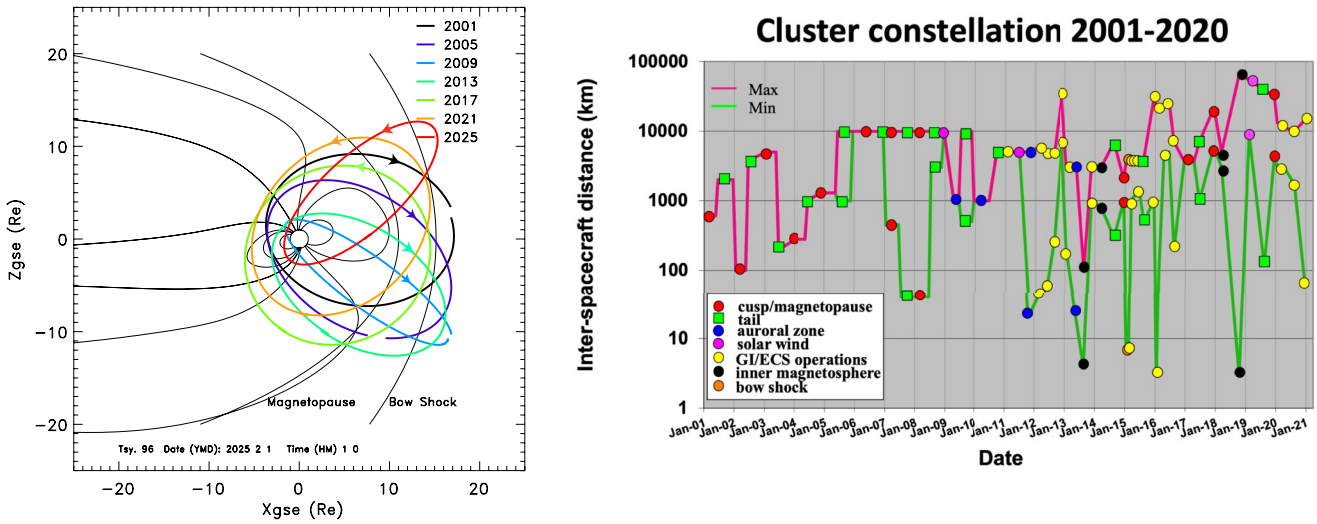

Figure 1. Dayside Cluster orbit evolution, predicted to 2025, and configuration strategy to the end of 2020 (from Escoubet et al., this issue).

the whole mission. For the early mission, a close, four-spacecraft array was maintained on an average spatial scale, which was changed through manoeuvres at the start of each mission phase. The spacecraft constellation evolved around the orbit, repeating every orbit within each phase between manoeuvres. Subsequently, in the later mission, more complex (multi-scale) operations were achieved in which two spacecraft had much smaller separation distances than the others (right hand of Figure 1). Nevertheless, all spacecraft have flown in formation throughout the mission. Currently, Cluster is entering its 21st year of full science operations.

As a result of this unprecedented data coverage of the magnetosphere, the wide range of analysis techniques have been continuously developed and applied in different ways to determine key quantities and investigate a large number of phenomena. An update on the application of these multi-spacecraft methods was documented in Paschmann and Daly (2008), and here we focus on magnetic gradients and specifically magnetic currents (e.g., Dunlop & Eastwood, 2008; Shen & Dunlop, 2008; Vogt et al., 2008). Below, we review the use of the curlometer method, in particular, covering its later adaptation to other recent missions (notably MMS, THEMIS and Swarm). The Magnetospheric Multi-Scale (MMS) mission is particularly notable since it follows Cluster in maintaining a close configuration for much of its orbit (Burch, Moore, et al., 2016), but on much smaller separation scales (a few km), while THEMIS has achieved a 3-spacecraft configuration (of the magnetospheric spacecraft) in its extended operations (Angelopoulos, 2008) and Swarm achieved 2 and 3 spacecraft formations at low Earth orbit (LEO) polar altitudes (Friis-Christensen et al., 2008) on meso-scales (∼100 km).

2. The Curlometer and Basic Developments

2.1. Method

The basic method to derive the electric current density, along with its various adaptions to different regions and conditions, has been reviewed in a number of past and recent papers. The standard application and early results of the curlometer based on Cluster was reviewed by Dunlop and Eastwood (2008), together with other Cluster based multi-spacecraft techniques, and this was followed by reviews of its adaptation in the ionospheric context (LEO) by Dunlop et al. (2020) and Trenchi et al. (2020) (and others in the ISSI book on ionospheric multi-spacecraft data analysis tools Dunlop and Lüehr (2020); as well as recently by Dunlop et al. (2018, 2021). Method implementations are in the Cluster Science archive (http://www.cosmos.esa.int/web/csa/software and see the technical note by Middleton and Masson (2016), and can be obtained ready to use.

The calculation uses four spatial positions in a non-planar configuration to make a linear estimate of the electric current density from Ampère's law, that is, $\mu_0 J = \mathrm{curl}(B)$, in regions of high electrical conductivity where the displacement current ($\mu_0\varepsilon_0\partial E/\partial t$) can be neglected (Russell et al., 2016), where B and E are the magnetic and electric fields and J is the current density. This curlometer technique (Dunlop et al., 1988; Robert et al., 1998),

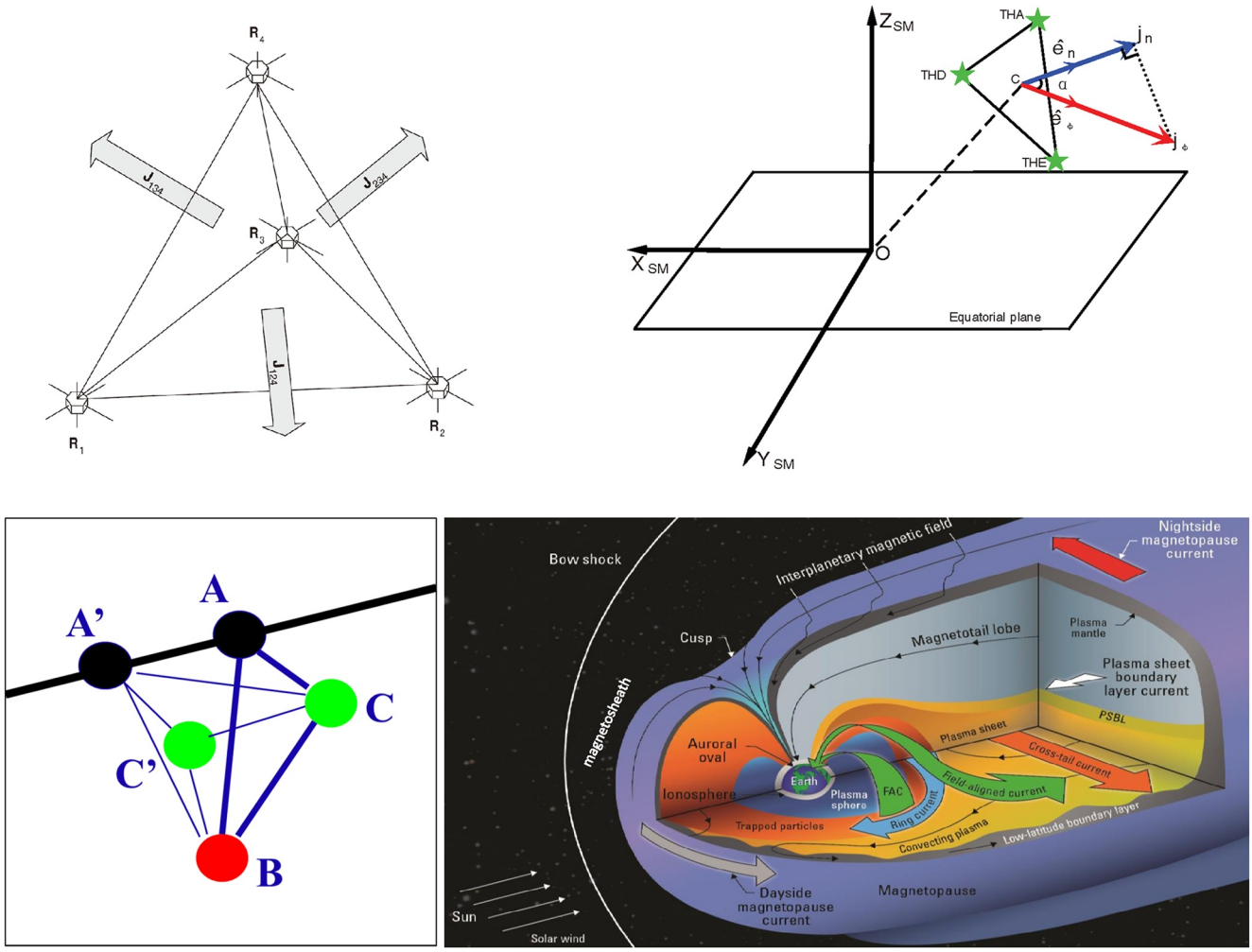

Figure 2. The curlometer concept (after Dunlop et al., 1988; top left); a configuration of the three THEMIS spacecraft in the ring current (from Yang et al., 2016, top right); a configuration of the three Swarm spacecraft (A, B, C) with adjacent positions (A', C') from a few seconds earlier (lower left), and a schematic showing some of the large-scale magnetospheric currents around the Earth (adapted from Kivelson & Russell, 1995, lower right).

therefore provides a rugged and simple formalism for the 3-D vector estimate of current density for a configuration of four spacecraft, that is, $\mu_0 \langle J \rangle . (\Delta R_i \Delta R_j) = \Delta B_i \Delta R_j - \Delta B_j \Delta R_i$, where ΔB_i, ΔR_i are the differences in the measured magnetic field and positions (i,j) to a reference spacecraft. The top left panel of Figure 2 represents the current density normal to each face of the spacecraft tetrahedron (the terms on the left hand side of the equation). In fact the fourth normal component is redundant and can be used to check stability of the estimate (Dunlop et al., 2018, 2020), by rotating the faces used to estimated J. (Note: this is particularly useful for highly irregular spacecraft configurations when the parameter Q is less useful as an quality indicator; see below).

Clearly, three of the spacecraft provide one component of J normal to that face of the tetrahedron and for very irregular spacecraft separations the relative alignment of the spacecraft configuration to the local field geometry is important, so that often only one face provides an accurate determination of the J component normal to that face (see also the note in Section 3.3 and the methodology in Shen, Rong, Dunlop, Ma, et al., 2012; Shen, Rong & Dunlop, 2012; Vogt et al., 2009). This partial estimate can still provide useful information when the large-scale current orientation is known, such as for field-aligned currents (Marchaudon et al., 2009), for example, and in the case of the in situ ring current (or the other large scale current systems shown in the lower right panel of Figure 2); as has been used to calculate ring current density primarily along the azimuthal component. With Cluster J components along the azimuth direction can be separated from the other components (Zhang et al., 2011), while with configurations of the three magnetospheric THEMIS spacecraft in the ring current (Yang et al., 2016), as

shown in the top right panel of Figure 2, the current density normal to the THEMIS plane can be projected into J_ϕ direction as shown. Swarm close configurations can also be used for partial current estimates. Where assumptions in the behavior of the currents can be made (e.g., the stationarity of the magnetic field, field-aligned or force-free structures), the curlometer can be generalized to extend the multi-point sampling using positions of the spacecraft at different times (Dunlop, Yang, Yang, Xiong, et al., 2015; Shen, Rong & Dunlop 2012; Ritter & Lühr, 2013; Vogt et al., 2013; and references in Dunlop & Lühr, 2020). Figure 2 (lower left) illustrates the adaption in Dunlop, Yang, Yang, Lühr, et al. (2015), where adjacent positions in time of the Swarm A, C satellites (A', C') are used to form at least four points in space, but at different times (limiting the useful cadence of the currents to the convection time across the array). The Swarm A, C pair fly side by side in near circular, polar orbits (~500 km altitude) for most of the mission (i.e., in the plane of the figure shown), while Swarm B flies at a slightly higher altitude (all 100–150 km apart). This means that time shifting A, C pair provides a non-planar configuration. In fact a series of estimates can be found using different combinations of the five points (A, B, C, A', C'), where ACA'C' provides a vertical (near FAC) component of J, while different four point selections (ABCA', etc.) provide a series of comparative estimates of the full vector current. The configuration ABC is of course a single time position, but suffers from the fact that the plane is not well aligned to the FACs. Changing the combinations allows slightly different parts of the current structure to be sampled so that some of the temporal and spatial nature can be probed. Both forward and backward time shifting can be applied.

Although robust, errors in the estimate arise from uncertainties in the magnetic field measurements, timing and the spacecraft separation distances; as well as from the form (scale-size, orientation relative to the spacecraft configuration) of the current structure (i.e., the neglect of nonlinear gradients in the calculation). For Cluster separations, typically (>100 km), the dominant error is that arising from nonlinear gradients, although measurement errors do contribute. Indeed, both Forsyth et al. (2011) and Runov et al. (2005) for example, have examined the effect of the characteristic size of current systems on the curlometer estimate. The linear estimator $Q = |\mathrm{div}B|/|\mathrm{curl}(B)|$, is useful as an indirect quality parameter (linked to the constellation shape and form of the magnetic field (Robert et al., 1998 and see also Haaland, Sonnerup, Dunlop, Georgescu, et al., 2004) and has been used extensively during Cluster studies (typically only to show when the curlometer estimate is likely to be bad). The linear estimate of the average value of div$B$ over the volume of the tetrahedron is an integral part of the method and is given by $\langle div(B)\rangle |\Delta R_i . \Delta R_j \wedge \Delta R_k| = |\sum_{\mathrm{cyclic}} \Delta B_i . \Delta R_j \wedge \Delta R_k|$, e.g., $\langle div(B)\rangle_{1234} (\Delta R_{12} \cdot \Delta R_{13} \wedge \Delta R_{14}) = \Delta B_{12} \cdot \Delta R_{13} \wedge \Delta R_{14} + \Delta B_{13} \cdot \Delta R_{14} \wedge \Delta R_{12} + \Delta B_{14} \cdot \Delta R_{12} \wedge \Delta R_{13}$.

This quality parameter can only be used for the full combination of the four positions so that the 2 and 3 spacecraft estimates for components of J, described above, do not have an indication of Q. In addition, Q is found to be unreliable if the spacecraft configuration is highly irregular and not well aligned to the background magnetic field structure. The estimate of Q has also been used in qualification of the FOTE (First-Order Taylor Expansion) method (Fu et al., 2015, 2016).

The effect of nonlinear gradients which are not associated with current density (first noted in Dunlop, Balogh, Glassmeier, et al., 2002; Dunlop, Balogh, Cargill et al., 2002; while Grimald et al., 2012; considered this more recently in the context of the ring current), can be minimized in the case of the Earth's magnetosphere by subtracting the dipole (or IGRF) field (for which the model current is zero, but the field gradients are non-linear) from the measured magnetic field to form magnetic residuals before applying the curlometer. This has been useful in studies of the in situ ring current (Yang et al., 2016), where the effect of the form of the dipole becomes significant, and the formation of magnetic residuals is normal practice in analysis of LEO data, particularly for Swarm (Dunlop et al., 2020; Ritter & Lühr, 2013). For the smaller scale MMS constellations the current density structure is usually well resolved, so measurement errors (in the magnetic field, spacecraft position and timing) become more critical, and typically these affect the estimate below a threshold $|J|$ (Dunlop et al., 2018). For the small MMS tetrahedron scales (a few km), measurement uncertainty (~0.1 nT in B; ~100 m for R and millisecond timing) drives the error unless the current density is greater than several nAm^{-2}).

2.2. Early Demonstrations

Many papers have used this technique with Cluster data across regions of the magnetosphere and in support of other derived quantities (see Section 5). Table 1 gives a summary of the values of current density typically found previously in the Earth's environment. These are based on the average large-scale morphology and transient structure typically found.

Table 1
Typical Current Density Values (Modified From Dunlop et al., 2018)

Feature/Region	Typical values for J
Magnetopause currents	~10 nA m^{-2} (Dunlop & Eastwood, 2008), to 100s nA m^{-2} (see e.g., Panov et al., 2008)
Currents in flux transfer events	~1 nA m^{-2} (Dunlop & Eastwood, 2008) up to 10 nA m^{-2} (Pu et al., 2005)
Current at the cusp boundaries	~20 nA m^{-2} (Dunlop, Balogh, Glassmeier, et al., 2002; Dunlop, Balogh, Cargill et al., 2002)
Field aligned currents (FAC)	~2 μA m^{-2} at 500 km altitude and ~20 nA m^{-2} at 2.5 R_E altitude. (Dunlop et al., 2005)
Magnetotail current sheet	up to ~30 nA m^{-2} (Runov et al., 2006)
Plasma sheet boundary layer	~10 nA m^{-2}, (Nakamura et al., 2004)
Ring current	9–27 nA m^{-2} at 4–4.5 R_E, (Zhang et al., 2011)
Solar wind current sheet	~10 nA m^{-2} (Eastwood et al., 2002)

Two key regions which lent themselves to the analysis most easily were the current sheets at the magnetotail and magnetopause (MP), which were targeted in early Cluster operations with the most regular tetrahedral configurations. Despite extensive studies the MP for decades, the four spacecraft Cluster mission made direct measurement of the vector current density possible for the first time. The magnetopause boundary layer (MPBL), in particular, was matched well to the spatial scale size in the initial mission phases (100–2,000 km spacecraft separation). Figure 3 summarizes the results of Dunlop and Balogh (2005) and Haaland, Sonnerup, Dunlop, Georgescu, et al., (2004). The top left figure shows that the J orientations lie predominantly in the MP plane during repeated crossings resulting from motion (average speed ~25 km/s; with average thicknesses ~1,200 km) back and forth arising from solar wind variations, usually in pressure (e.g., Sibeck et al., 1991). Typically, the Earth's magnetopause may vary in thickness from 100s of km (a few ion gyro radii) to 1000s of km (Berchem & Russell, 1982; Paschmann, Halland, et al., 2005; Paschmann, Schwartz, et al., 2005; Panov et al., 2008), while corresponding current densities vary from 10–100 nA/m^2 (high-intensity, small-scale sub-layers were not often resolved by Cluster, as shown in Section 5). The signatures with different orientations outside the main MP crossing period were identified as magnetosheath FTEs (see Section 4.2), where the current is along the mean reconnected flux tube direction (also studied by Pu et al., 2005).

The combination of the curlometer and discontinuity analysis to obtain the boundary orientation and motion (see Dunlop and Woodward, 1998; Dunlop, Balogh, Glassmeier, et al., 2002; Haaland, Sonnerup, Dunlop, Balogh, et al., 2004) can confirm the MP thickness, relative to the scale of the configuration, and alignment of J in the local MP plane, even in the presence of ripples on the MP boundary tied to the current density orientation (top right). Broad scaling of the current density (ranging from 10–50 nAm^{-2}) with MP thickness can be shown to be crudely consistent with the effective Chapman-Ferraro current $(\Delta B/\Delta D)/\mu_0$, as shown in the bottom left of Figure 3. The cluster result tends to under estimate the current for higher J and thicker boundary layers (compared to the separation).

The MP was also shown to be as thin as 200 km for some crossings (bottom right), where application of the MVAJ method (see also Xiao et al., 2004; who apply the method to FTE orientations) allows the orientation of the current sheet to be better tied to J (minimum variance of J is used to obtain the orientation of a near 1D current sheet, since div $J = 0$, when $\mu_0 J = \text{curl } B$). The velocity of the current sheet can also be obtained from the relations given in Haaland, Sonnerup, Dunlop, Georgescu, et al. (2004) and the different estimates of orientation all agree to within a few %.

2.3. Adaption to LEO Data: Use of Time Stationarity

Multi-point measurements suitable for the curlometer at low-Earth orbit (LEO) altitudes only became possible after the launch of the three Swarm spacecraft in 2014. In fact, the curlometer can be generalized (using nearby positions in time as indicated in Section 2.1) to provide estimates in this region (i.e., even when only 2 or 3 spacecraft are closely separated) under the assumptions that either the dominant currents are field-aligned in the high ionosphere and thermosphere, or that the characteristic currents do not evolve on suitable, short time-scales (Dunlop, Yang, Yang, Lühr, et al., 2015; Dunlop, Yang, Yang, Xiong, et al., 2015; Ritter & Lühr, 2006, 2013;

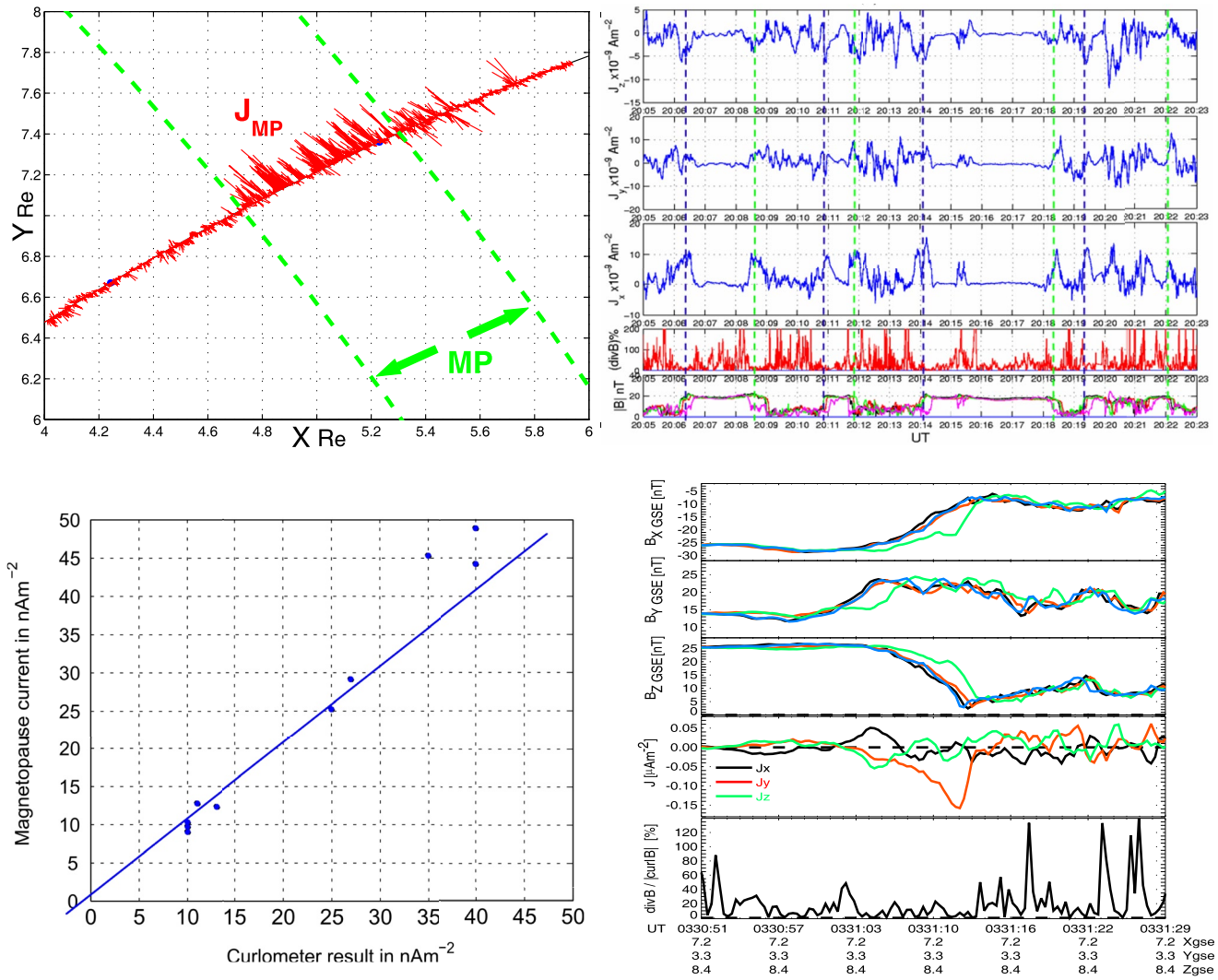

Figure 3. (top left) Projected current density vectors from the Curlometer for the period of repeated MP traversals on the January 26, 2001, as Cluster moves outbound through repeated in-out motions of the MP and into the magnetosheath. (top right) The MP current density, showing changes in orientation which follow the MP orientation during a series of ripples or large scale boundary waves (lower panels are the value of Q and the multi-spacecraft magnetic field magnitude). (bottom left) Comparison of the magnetopause current density estimated from an equivalent Chapman-Ferraro sheet to the curlometer for a range of crossings (from Dunlop & Balogh, 2005). (bottom right) Plot of the multi-spacecraft plasma density, magnetic field and current density, with values of Q at the bottom, for a thin magnetopause (on March 2, 2002), where the spacecraft separation was ∼100 km. Estimated current densities reach 160 nAm^{-2} and calculated from MVAJ as extending over 200 km (from Haaland, Sonnerup, Dunlop, Georgescu, et al., 2004).

references in Dunlop & Lühr, 2020). The subtraction of the main field components prior to the application of the method is essential at LEO altitudes (400–600 km) since the Earth's internal field dominates (in the examples below we subtract the Chaos model field (e.g., Olsen et al., 2014) to compute the magnetic residuals). Any time dependence in the current signatures is usually assumed to be at higher frequencies than the typical convection time of the currents across the spacecraft array. For Swarm configurations, the spacecraft separation is ∼100–150 km at mid to high latitudes, corresponding to a suitable time lag of ∼10–15s, so that low pass filtering of the currents is suitable to obtain consistent estimates. If the (field-aligned) current systems are highly time dependent (e.g., in the case of ULF or Alfvén waves) then this filtered, multi-spacecraft estimate will be less meaningful; but in fact high time dependence is usually associated with small scale currents, so that the individual spacecraft measured field will typically be different at each spacecraft in those cases. The extended methodology is therefore useful to map out the morphology and dynamics of the larger scale current systems, such as the region 1, region 2 and

NBZ FAC systems (see reviews in Cao et al., 2010; McPherron et al., 1973; Shiokawa et al., 1998), and at least can indicate the occurrence of smaller scale and time dependent structures.

Figure 2 (lower left) shows the configuration of the Swarm A, B, C spacecraft for an event considered in Dunlop, Yang, Yang, Xiong et al. (2015), which in fact provided a close conjunction of Cluster and Swarm (as shown in Figure 4) and produced a series of 2, 3 and 4 spacecraft estimates for the FACs sampled by Swarm. The 4-spacecraft combinations also allow calculation of Q, which has very low values (a few %) during the periods of significant current density. Changing the choice of spacecraft positions can show how stable the current is, since the mean times (the effective barycentre) of each set of four positions are all slightly different. We can compare the field-aligned component obtained from the 4-point calculation to that of the normal component (from the shifted AC pair), and also to the filtered single spacecraft FAC estimates from *dB/dt* (see Lühr et al., 2015), in order to check the field-aligned signatures (as shown on the right of Figure 4). These comparisons show that the FAC profiles obtained from the 4-point estimates match those from Cluster most closely (with suitable scaling). The Cluster traces show the progressive approach to the highest MLAT values (dark blue portion of the lower panels), where the Cluster tracks cross the local time of the Swarm orbit (within minutes of the Swarm pass). The implication of the results is that structures on scales of 1–200 km (at LEO altitudes) are can be coherently mapped between Cluster and Swarm altitudes.

An additional effect of applying the 4-point calculation is that any perpendicular components can be found. It isn't clear whether at Swarm altitudes perpendicular current would be suppressed but estimates for this event have shown stable signatures characteristic of associated hall signatures for wire model FACs (see, Gjerloev & Hoffman, 2002; Liang & Liu, 2007; Ritter et al., 2004; Shore et al., 2013; Wang et al., 2006). Various closely related methods using groupings of the spacecraft at the high latitude regions of LEO have been compared in an

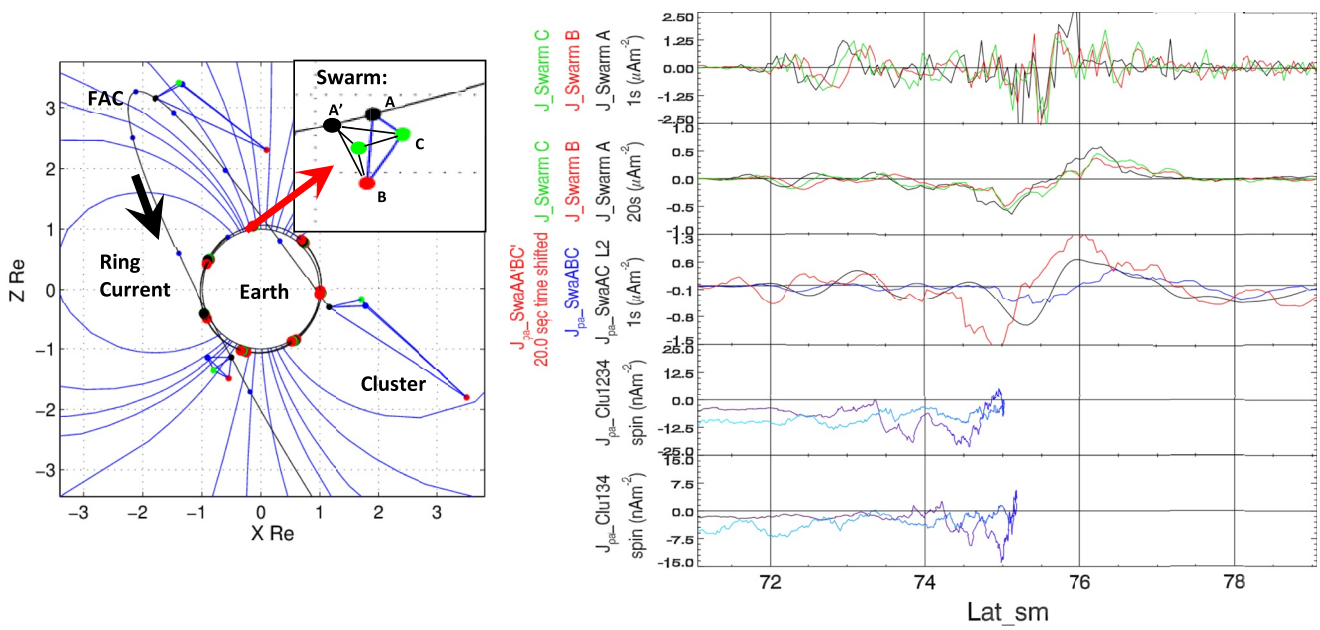

Figure 4. Conjunction of Cluster and Swarm, taken from (Dunlop, Yang, Yang, Xiong, et al., 2015), showing the orbits projected into Z,X_{GSM} (left panel). Model geomagnetic field-lines are shown for guidance, while configurations of the Cluster spacecraft are plotted relative to the orbit track of C1 and are enlarged by a factor of 3. Cluster moves from the dusk (front) side to high-latitudes (marked FAC) and then across the dawn side through the ring current. The Swarm orbit lies close to Z,X_{GSM} and the satellites pass under the Cluster orbit and across the polar cap in the minutes around the high-latitude position of Cluster (the inset shows zoomed views of the Swarm configurations, enlarged by a factor of 5 relative to the orbit of Swarm A). The magnetic footprints of Cluster cut across those of the Swarm orbit within minutes of Swarm passing over, where the Cluster track moves from lower latitudes though the expected R2 boundary into the auroral region and back to lower latitudes. (right) Plot showing the Swarm and Cluster FACs as a function of MLAT. The top two panels show the estimates for the unfiltered and 20s filtered, single spacecraft FACs (for Swarm A, B, C), while the middle panel shows the different Swarm multi-spacecraft estimates (the 4-point method is in red; the FAC projection estimated from the ABC planar configuration is in blue, and the smooth black line is the level 2 duel spacecraft estimate). The bottom two panels show Cluster FACs estimated for only the face perpendicular to the magnetic field, as well as for the full curlometer. The light blue trace corresponds to the times after the conjunction as Cluster moves back to lower latitudes at different local times.

assessment of key events by Trenchi et al. (2020). A time shifted configuration, tailored to the low latitude regions covered by Swarm has also been applied to extract low latitude currents (Fillion et al., 2021).

3. Magnetic Field Gradients and Topology: Extraction of *J*

The magnetic field measurements on board multiple, formation flying spacecraft more generally allow both the gradient and curvature terms in the dyadic of the magnetic field, *B*, to be linearly estimated (Chanteur, 1998; Harvey, 1998a, 1998b; Shen & Dunlop, 2008; Shen, Rong, Dunlop, Ma, et al., 2012; Shen, Rong & Dunlop, et al., 2012; Vogt et al., 2008), from which the current density can be extracted; usually employing a formalism in barycentric coordinates (for *J* this is identical to the form in Section 2, but the error handling is slightly different). A full set of gradient terms can be obtained with an array of at least four spacecraft. Key formulations of this methodology are magnetic curvature and rotation analysis (Shen et al., 2007, Shen, Rong, Dunlop, Ma, et al., 2012; Shen, Rong & Dunlop, et al., 2012) and least squares analysis applied to planar reciprocal vectors (De Keyser et al., 2007; Hamrin et al., 2008; Vogt et al., 2009, 2013). The performance of these related gradient methods, in general, depends on the integrity of the spacecraft array and the stationary properties (temporal dependence) of the magnetic structures, although additional constraints for some structures can be added.

3.1. Magnetic Rotation Analysis Applications

The methods of Magnetic Curvature Analysis (MCA) (Shen et al., 2003) and Magnetic Rotation Analysis (MRA) (Shen et al., 2007) were reviewed in Shen and Dunlop (2008). The 3-D topology of magnetic field (curvature radius, normal direction and binormal direction of the magnetic field-lines), as well as the direct gradients, can be deduced, and the method has also been applied to the magnetotail current sheet (Shen, Liu, et al., 2008, Shen, Rong, et al., 2008; Rong et al., 2011), the Earth's ring current (Shen et al., 2014) flux ropes and plasmoids (Yang et al., 2014; Zhang et al., 2013), reconnection regions (Lavraud et al., 2016; Zhang et al., 2016) and at the cusp and magnetopause (Shen et al., 2011; Xiao et al., 2018).

Figure 5 (left) shows estimates of the field-line curvature (from MCA) in the ring current, relative to the implied curvature from the Earth's dipole field. This can infer the current strength at those locations in a broad sense and therefore is complimentary to the calculation of *J* from the magnetic gradients. The growth of the implied current density (decrease in relative curvature) with geomagnetic activity (SYM-H) and the apparent dawn-dusk asymmetry, particularly during lower activity levels, can be seen in the plot. Figure 5 (right) shows another application indicating that the form of the tail current sheet has three types (the normal, the flattened, and the tilted), as discussed in detail in Rong et al., (2011). These distinct geometries are implied by the combined MCA/MRA methodology, through the extraction of the key properties of the curvature radius, normal direction and binormal direction, and have significance for current sheet dynamics.

3.2. Least-Squares Methods for Multi-Point Gradient Computation

In many situations (for instance, with Cluster) the instruments record multiple data points in the time span needed for the spacecraft to cover a distance comparable to the typical separation scales. Intuitively, all those measurements carry information that may be relevant for the calculation of the gradient, as was already noted by Harvey (1998a, 1998b); particularly if a certain degree of invariance of the structures of interest, as a function of time, can be assumed. This is the idea behind the Gradient Analysis by Least-Squares (GALS) technique (Hamrin et al., 2008), and a similar method (LSGC), also based on a least squares gradient calculation. The Least-Squares Gradient Calculation (LSGC) technique (De Keyser et al., 2007; De Keyser, 2008) approximates the quantity to be measured (scalar or vector) with a Taylor series expansion around the point of reference in space and time (typically the barycenter of the set of measurement points). The expansion describes the field in terms of the value at the reference point, its space and time gradients, and higher-order nonlinear terms; it can be assumed that the homogeneity scales over which the gradient can be considered constant are known, so that higher-order terms can be estimated (the procedure can be applied iteratively, solving in a weighted least-squares sense). The method provides error estimates on the results, reflecting both the measurement errors and the errors that stem from the non-linear behavior of the gradients. In the simplest case, the measurement errors are taken to be uncorrelated. A further simplification can be made by assuming that the homogeneity parameters are the same for the three

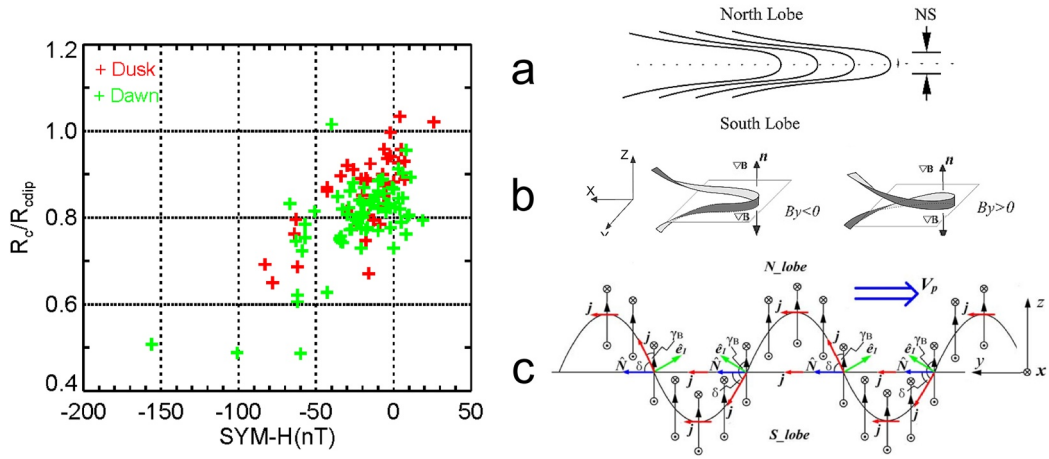

Figure 5. (left) Field-line curvature relative to that of the model dipole field for a set of ring current crossings sampled by Cluster (Shen et al., 2014), where dusk and dawn locations have different colors. (right) Cartoon of the types of field topology (Rong et al., 2011) found in the cross tail current sheet: (a) normal current sheet, (b) flattened current sheet (c) tilted current sheet.

components. Constraints (e.g., that the gradient along the magnetic field is zero, $divB = 0$, and that the structures are static, but not stationary) can be added. The method then provides the magnetic field components and their space and time derivatives, from which one can compute the curl and the divergence. Since divergence and curl combine terms of the same order of magnitude, possibly with opposite sign, the relative error on the result can be large. Note also that such errors typically are anisotropic. If the time variability of the electric field can be neglected, the current density is readily computed from the curl.

These techniques can in principle be applied to measurements provided by an arbitrary number of spacecraft, although in practice the quality of the results depends on the measurement errors. When the set of measurement points is sufficiently rich (multiple spacecraft, well-spaced, sufficient time resolution) LSGC can exploit significantly more data than the classical curlometer (a special case of LSGC), leading to a more reliable result. An interesting aspect is that LSGC also provides a total error estimate on the current density that includes the contributions due to measurement error and to the non-linearity of the field variations.

3.3. Irregular Tetrahedron Shape

It is worth noting here that the conventional ways to calculate the gradient involve the calculating of the inverse of volume tensor (e.g., Chanteur, 1998; Harvey, 1998a, 1998b; Shen et al., 2003, 2007). The volume tensor would become an ill-matrix, however, when Cluster tetrahedron becomes an irregular shape, for example, plane-like or line-like, so that the direct calculation of the inverse of volume tensor would yield significant error and gradient cannot be correctly calculated in this case. To avoid the dilemma, Shen, Rong, Dunlop, Ma, et al. (2012) presented a procedure in order that the gradient can be universally calculated if one transforms the coordinates into the eigenvector space of volume tensor. Shen, Rong, Dunlop, Ma, et al. (2012) successfully applied their method to the three-point observation of THEMIS to calculate the current density and the vorticity of plasma flow, and also to the three-point plasma measurement of Cluster to calculate the vorticity of K-H waves.

4. Application by Regions

Due to its robust and flexible nature, the curlometer calculation is perhaps the most widely used in the magnetosphere (notably applied in: the magnetopause boundary layer (e.g., Dunlop, Balogh, Cargill, et al., 2002, 2005; Haaland, Sonnerup, Dunlop, Georgescu, et al., 2004; Panov et al., 2006, 2008; Shi et al., 2019); the magnetotail (e.g., Runov et al., 2006; Nakamura et al., 2008; Narita et al., 2013); the ring current (e.g., Shen et al., 2014; Vallat et al., 2005; Yang et al., 2016; Zhang et al., 2011); field-aligned currents (e.g., Dunlop and Lühr, 2020; Forsyth et al., 2008; Marchaudon et al., 2009; Shi et al., 2009, 2010, 2011) and other transient signatures and in the solar

wind (e.g., Eastwood et al., 2002; Roux et al., 2015; Shen, Liu, et al., 2008; Shen, Rong, et al., 2008; Eastwood et al., 2002; Xiao et al., 2004). Below, many applications and studies using the curlometer are summarize region by region.

4.1. Magnetopause Current

The Earth's magnetopause (MP) forms a current sheet between the magnetic fields in the magnetosheath and magnetosphere, and thus is a key region for the mass, momentum and energy to be transferred from the solar wind into the magnetosphere (see Harland et al., this issue for a review of Cluster results). Based on the application of the curlometer method to Cluster observations, macroscale current density features of the magnetopause have been shown (e.g., Dunlop & Balogh, 2005; Haaland & Gjerloev, 2013; Haaland et al., 2014; Maynard et al., 2003, 2005, 2012; Panov et al., 2006, 2011; Phan et al., 2004; Pu et al., 2005; Tang et al., 2012), typically carried out for thicknesses of the MPBL ranging from 1-2 R_E down to a few hundred kilometers. It has also been used in studies of the cusp (Dunlop et al., 2005; Khotyaintsev et al., 2004; and see Pitout and Bogdanova, this issue), and to determine flux-rope properties at the magnetopause (Xiao et al., 2004; Zuo et al., 2004), and at high latitudes (Thompson et al., 2004). A summary of these studies is given in Paschman, Schwartz, et al., (2005); Paschman, Halland, et al., (2005).

Figure 6 (left) shows statistical results of magnetopause current on the low latitude flank (Haaland & Gjerloev, 2013; Haaland et al., 2014). The results show that the average current densities on the dusk-side (~42 nAm^{-2}) are higher than dawnside (~35 nAm^{-2}), although the dawn-side values dominate at low current density, and this dawn-dusk asymmetry cannot be fully explained by solar wind conditions. Haaland et al. (2014) suggested these results implied both asymmetries in the magnetosheath and the geometry of the bow-shock, and/or ring current asymmetries for the larger current densities (see right-hand schematics in Figure 6). The curlometer values of J were ~40% higher than $\Delta B/d$.

For many crossings, detailed current density forms indicate that two or more adjacent current sheets can exist at the magnetopause, each current sheet often having different current directions and being several ion gyroradii in thickness, typically (Haaland, Sonnerup, Dunlop, Georgescu, et al., 2004). A more complex structure at the flank magnetopause than a thin, one-dimensional current sheet (described by a Chapman-Ferraro layer) is therefore often present, although such substructure can only be resolved with Cluster for the smallest separations and the plasma structure is nominally limited to spin (4s) time resolution (see also Section 5). Indeed, the first curlometer results reported by Dunlop, Balogh, Glassmeier, et al. (2002); Dunlop, Balogh, Cargill et al. (2002), showed that an event from the cusp region had two distinct peaks in the current density. Such layered current sheets are also seen in kinetic tangential discontinuity models (e.g., Roth et al., 1996).

4.2. The Earth's Ring Current (Cluster, THEMIS and MMS)

The terrestrial ring current (RC) is a large region where the curlometer has also been applied (Dandouras et al., 2018; Dunlop et al., 2018), which is variable in strength, extends radially from about 2–7 R_E and often extends from −30 to 30° in latitude. It has also been used to determine spatial gradients in the plasmasphere (Darrouzet et al., 2006; De Keyser et al., 2007). Cluster generally crosses the ring current every perigee pass so extensively sampled the region in local time and latitude, but for a narrow range of radial distance (~4–4.5 R_E): giving in situ current densities directly. As first reported by Vallat et al. (2005), Cluster in its polar orbit cuts nominally north to south through the ring plane and allows all local times to be scanned (Zhang et al., 2011), as shown on the left hand side of Figure 7. The Cluster configuration is oriented in such a way that it typically allows an accurate estimate of the azimuthal (ring plane) current density component, J_ϕ, to be made. The effect of non-linear spatial gradients in the Earth's internal field in this region, is reduced by first subtracting the IGRF from the measured data to form magnetic residuals, to which estimates of the current density are applied (see Section 2). In general, there is a strengthening of the RC with storm activity together with a dawn/dusk asymmetry. A possible relation between asymmetries in the RC and those at the MP have been suggested by Haaland & Gjerloev (2013).

The three magnetospheric THEMIS spacecraft also achieve coverage of a wide range of MLT (Yang et al., 2016), while in a close configuration (see top right of Figure 2), as shown in the middle of Figure 7. The dawn-side

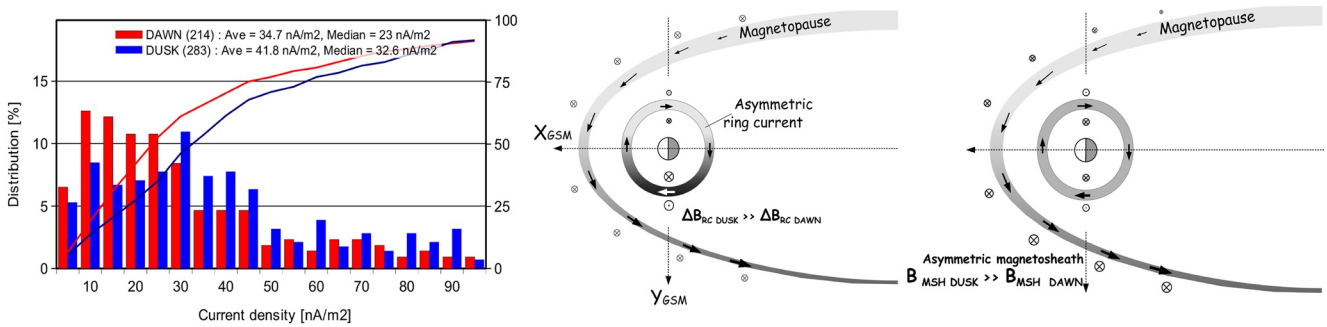

Figure 6. (left) Curlometer results showing the magnetopause current distribution. Histogram bins are 5 nA/m^2 wide. Cumulative values are indicated by the lines (scale is the right hand vertical axis). Lower current densities occur for dawnside MP crossings for higher current densities (Haaland, Sonnerup, Dunlop, Georgescu, et al., 2004). (right) schematics of the asymmetric MP current density for either an asymmetric RC or magnetosheath. The total current is constant since the MPBL thickness larger on the dawn-side.

coverage in MLT is limited so that the trends are not fully resolved. The radial (i.e., L-shell) profile for the recovery phase of each storm period can be revealed, however, and the reversal in Westward-Eastward current on the inner edge of the RC can be identified (at $\sim L = 5$ on average, but is sensitive to storm activity; ranging from 4–5.5 R_E), as shown on the right panel of Figure 7. The MMS spacecraft also samples the ring current in a near equatorial orbit (but on the smaller MMS scales), which limits latitude coverage but also covers a wide range of radial distance. Comparisons may be made with Cluster measurements, so the two missions are complement each other, both in spatial resolution and emphasis on the region covered. Thus, MMS can better resolve the trends seen in both the radial and azimuthal morphology, and also can identify small scale intense currents, which are not resolved by Cluster or THEMIS.

4.3. The Magnetotail Current Sheet and Dipolarization Front

Both current structure and stability of the magnetotail current sheet is perhaps the most investigated in the magnetosphere, as it can affect the overall dynamics of the magnetosphere. It is thus also an important region where the curlometer method is widely used (see Nakamura et al., this issue), covering topics such as its basic structure, dynamics, and (surface) waves (Runov et al., 2006; Rong et al., 2011; Thompson et al., 2006; Takada et al., 2006; Volwerk et al., 2003; Zhang et al., 2006), and (sub)structures formed during substorm disruptions (Henderson, Owen, Alexeev, et al., 2006; Kivelson et al., 2005; Laitinen et al., 2007; Lui et al., 2007; Nakamura et al., 2006, 2018; Xiao et al., 2006). The application to field-aligned currents in the magnetotail plasma sheet boundary layer will be introduced in Section 4.5.

Using four-point magnetic field measurements by the Cluster spacecraft, Runov et al. (2005, 2006) statistically analyzed rapid magnetotail current sheet crossings observed in July–October 2001. They distinguished three types of current sheet distributions: central (classical Harris type) current sheets (I) with a sharp, symmetric maximum; bifurcated, quasi-symmetric current sheets (II) with maxima north and south, and non-centred asymmetric sheets (III) (Figure 8, left panel). In fact, non-Harris-type behavior is typical as confirmed by plasma distributions, that is, a thicker plasma sheet contains internal current peaks. The type I sheets are typically thinner (~2,000 km) compared to type II (~4,000 km). The kinetic structure of embedded, thin horizontal currents has also been investigated (Artemyev et al., 2009). Indeed, Artemyev et al. (2013, 2015) have investigated intense thin current sheets observed by Cluster in the later (2003) phase and compared the results of the curlometer with particle currents, to show that electrons often carry almost the entire current and the most current densities are contributed by electron curvature currents. Furthermore, the most intense currents are observed under disturbed conditions (i.e., in the vicinity of magnetic reconnection). The orientation and current density of the current sheet and its relationship with geomagnetic conditions was analyzed statistically from Cluster's 2001–2007 tail seasons data (Davey et al., 2012). Flapping current sheet motion has also been revealed (e.g., Zhang et al., 2006), thought to be associated with kink-like surface waves, with wave fronts which are tilted in the Y−Z plane and move out on either side of the central magnetotail. Complementary analysis has been shown in Section 3.1, where the MRA analysis confirmed different current sheet geometries associated with various flapping modes (Rong et al., 2011; Shen et al., 2003).

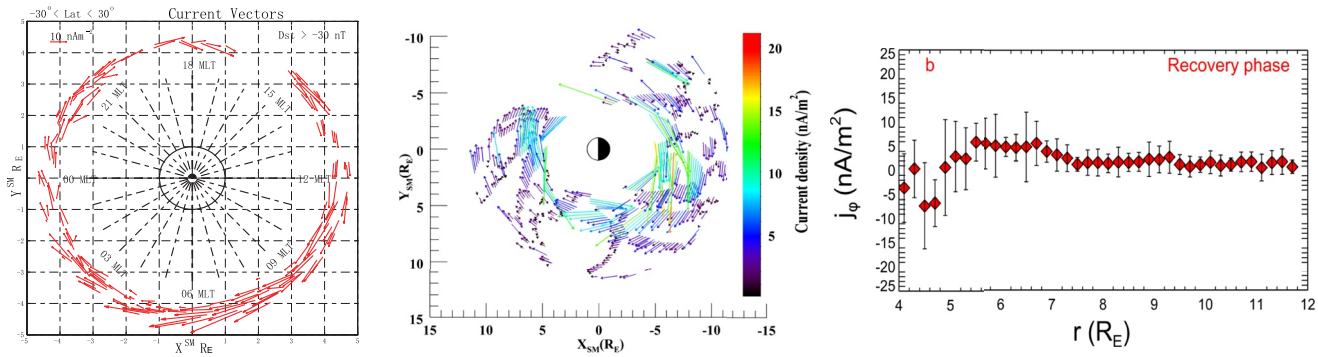

Figure 7. (left) Magnetic local time (MLT) scan of Cluster ring current (RC) passes, plotted in solar magnetic (SM) coordinates, and between −30° to 30° latitude (after Zhang et al., 2011). Averages (10 min) of the current density obtained from the curlometer are shown by the length and direction of each arrow. The measurements represent non-storm (Dst > −30 nT) values of the RC. There is an overall increase in J_ϕ from 03–12 MLT on the dawn-side while it remains low on the dusk side. (middle) Current densities projected into the ring plane are shown in a similar way (from THEMIS) for all storm activities during the recovery phase, showing the wider range of radial coverage achieved (for about 4–12 R_E) and an enhanced current near midnight LT for storm events. (right) Radial profile of the current density from THEMIS measurements.

Transient structures, related to the relaxation of magnetic field lines following sub-storm onset, dipolarization fronts (DFs), which are transient magnetic boundaries embedded inside the (Earthward) high-speed plasma flows, have also been studied with the curlometer. These boundaries separate hot tenuous plasmas from the cold dense plasmas in the magnetotail (Nakamura et al., 2002; Runov et al., 2009). The curlometer analysis indicates that, at the boundary of the dipolarization front, structures exist on scales below the proton gyro-scale. Also, for DFs with preceding dips, Yao et al. (2013) showed from Cluster that, dawn-ward currents exist in the dips, but are dusk-ward within the DFs. In the absence of preceding dips, there are only dusk-ward currents within the DFs. Furthermore, they also showed that the presence of dawn-ward, and mainly parallel, current in those DF which were preceded by dips is important for current driven M-I coupling. The field-aligned currents near the DFs seen by Cluster were also statistically studied by Sun et al. (2013), who found that these FACs have dimensions characteristic of the DFs, with a region-1 current direction within the DF and region-2 direction within the preceding dips. These Cluster observations indicate that the DFs can carry strong field-aligned currents and can appear as small "wedgelets" in the magnetotail (by analogy to the SCW, Liu et al., 2013, 2015), thus contributing to the substorm current system. Recently, using the MMS spacecraft with smaller separation, Liu et al. (2018) found the existence of an electron-scale current within the DFs (Figure 8, right). Furthermore, parallel currents only exist on the high-density side of the DFs (Figure 8, right panel "e"), rather than being uniform across the whole DF layer as suggested by previous studies.

4.4. The Magnetosheath and Solar Wind

In the upstream solar wind, the Curlometer has also been used to determine J in current sheets on a variety of scales, as well as through the heliospheric current sheet (Dai et al., 2014; Eastwood et al., 2002), and at the quasi-perpendicular bow shock, the method has also enabled the investigation of the cross shock electric field (Eastwood et al., 2007), and other large scale structures, as well as for intense current sheets (Artemyev, Pritchett, et al., 2018; Artemyev, Anton, et al., 2018). Thin current sheets have also been seen in the magnetosheath (Chasapis et al., 2015; Yordanova et al., 2016).

In these turbulence plasma environments, however, a variety of other coherent structures (on smaller scales) have been successfully detected on basis of the curlometer analysis. For instance, apart from the heliospheric current sheet and other current layers, magnetic islands, magnetic holes, mirror mode structures, shocks, solitons, are recognized in the solar wind, magnetosheath, and magnetotail (Huang et al., 2016; Hau et al., 2020; Maynard et al., 2008; Perrone et al., 2016, 2017; Vörös et al., 2017; Wendel & Adrian, 2013). It is important to note the existence a specific type of structures, namely, the Alfvénic structures, which exhibit correlations between magnetic field and velocity field fluctuations (Perrone et al., 2016). The application of curlometer on magnetic field/velocity field have allowed the estimation of current density/vorticity, thus facilitating the identification of Alfvén vortices and coherent and compressive current layers in above areas (Perrone et al., 2016, 2017; Wang

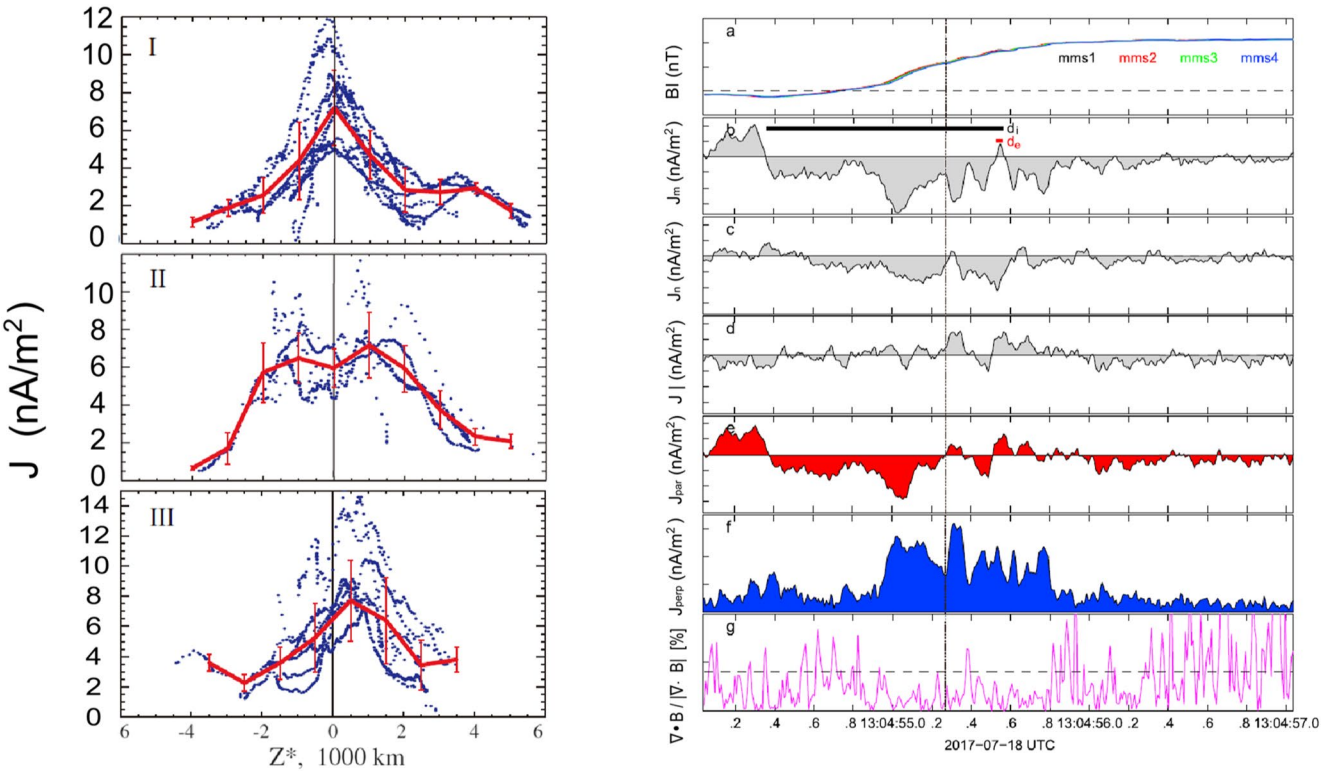

Figure 8. (left) Dependence of the magnetotail current |J| in nA/m^2 on the distance above and below the neutral sheet for individual crossings (blue dots) and binned averages (red lines). The data are classified as three different characteristic types of current sheet (from Runov et al., 2006). (right) MMS observation of the structure of J on electron-scales around a DF in boundary normal coordinates. The top four panels show the 4-spacecraft B_l magnetic field components and the current density (as N,M,L components). Local inertial lengths for ions and electrons is indicated as black and red bars in panel (b). Panels (e) and (f) show the parallel/perpendicular J components. Panel (g) shows the Q parameter. The high-density to low-density boundary across the DF layer is indicated by the black dashed line (adapted from Liu et al., (2018).

et al., 2019). Flow vortices have also been observed in the Bursty Bulk Flow of the plasma sheet based on analysis of vorticity and its anisotropy (Zhang et al., 2019, 2020). Kelvin-Helmholtz vortices have been identified in the dawn flank of the magnetosphere (Settino et al., 2021).

Figure 9 shows an example of Alfvén vortex in the magnetosheath. This nonlinear structure is characterized by coherent magnetic and velocity fluctuations mainly in the perpendicular plane with respect to the background magnetic field (Alexandrova et al., 2006; Alexandrova, 2008). As demonstrated in Figures 9a and 9b, the perpendicular magnetic field and velocity field fluctuations are well correlated, indicating the Alfvénicity of the structure. Moreover, the dominant parallel current (red curve in Figure 9c) is also negatively correlated with the dominant parallel vorticity. The 2D cylinder shape of the Alfvén vortex are illustrated in Figure 6e, emphasizing the parallel current density layers. The quasi-monopole of model and the relative MMS spacecraft trajectory are plotted in Figure 9f.

4.5. FAC in the Magnetosphere

The curlometer technique can measure FACs in the magnetosphere, both on Cluster separation scales in regions up to several R_E from the Earth and at LEO (i.e., at altitudes from 400 to several hundred km), as sampled by Swarm (Dunlop, Yang, Yang, Lühr, et al., 2015; Dunlop, Yang, Yang, Xiong, et al., 2015), as summarized in Section 2.3. The technique has also been applied to the magnetotail plasma sheet (Artemytev, Pritchett, et al., 2018; Artemytev, Anton, et al., 2018; Cheng et al., 2016; Chen et al., 2019, 2021; Nakamura et al., 2004, 2018; Shi et al., 2009, 2010) and to particular events in the plasma sheet boundary layer (Shi et al., 2009, 2010). The latter study showed that estimates of J from both the curlometer and particle moments agree and that the currents are carried by electrons (see Figure 10). It has also been shown by Forsyth et al., 2008; that FACs are present in

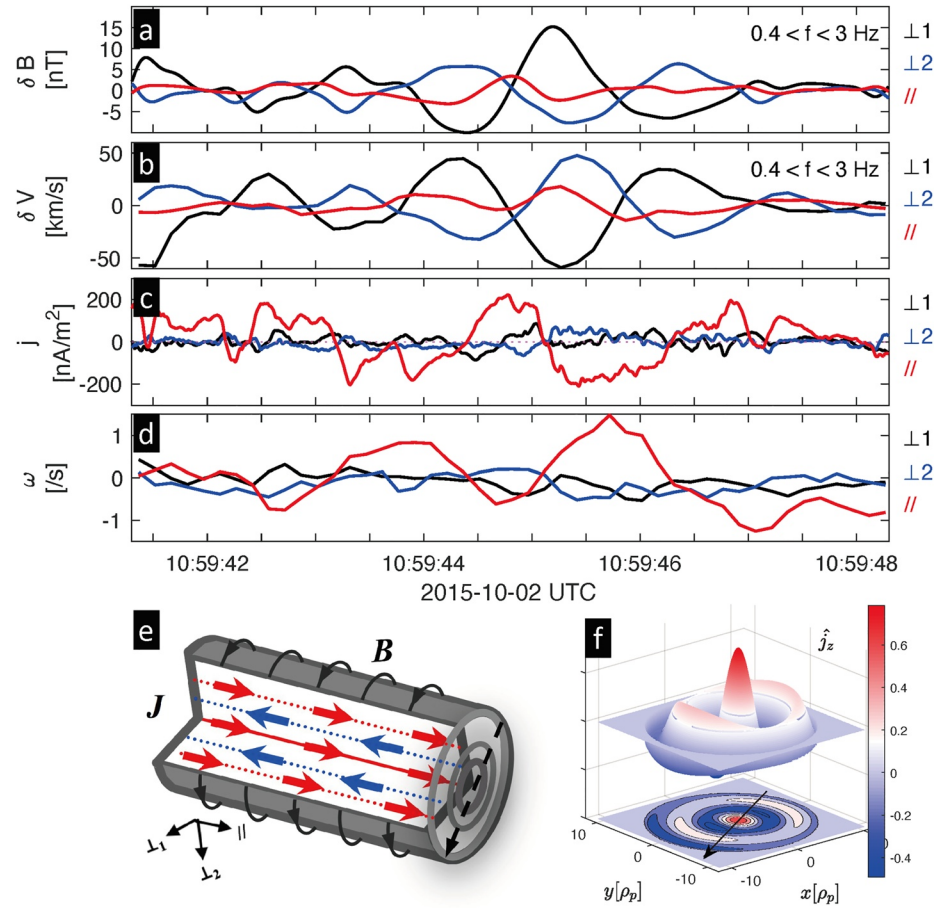

Figure 9. Example of an Alfvén vortex discovered by MMS. The magnetic field and velocity field are bandpass filtered at the frequency range around ion scales (0.4–3 Hz). The 2D vortex is comprised of dominant parallel current and vorticity with respect to the background magnetic field. The spacecraft is supposed to record major perpendicular magnetic field and velocity fluctuations when it passes through the cross section of the vortex. Furthermore, it should witness the parallel current density/vorticity based on multi-spacecraft reconstruction of the current density/vorticity through curlometer method. The Figure is adopted from Wang et al. (2019).

bursty bulk flows in the magnetotail and FACs have also be shown to operate in connecting the magnetotail to the ionosphere (Amm et al., 2005; Cheng et al., 2007). Parallel currents (and their particular current carriers) also can be accessed in the magnetopause boundary layers (see Section 5 for MMS studies) and in FTEs and other flux tubes (see Section 4.7).

4.6. Energy Conversion, Hall Term and Wave-Particle Interactions

The curlometer has also been applied to examine the $J \times B$ term (Hall term) in the generalized Ohm's law (which corresponds to differential motion between the ions and electrons, and curlometry has shown to be a key tool in understanding this term and is essential to understand the physical process of sub-ion structure). Curlometry can therefore progress our understanding of a range of processes in, for example, the normal electric field structure of collisionless shock (Eastwood et al., 2007); the $J \times B$ force associated with bursty bulk flows (Karlsson et al., 2015); encounters with the ion diffusion region (Tobert et al., 2016), where the ion plasma is not frozen to the magnetic field, and the dipolarization front created by magnetotail reconnection (e.g., Fu et al., 2012). It has also been employed in this respect to examine the extent to which magnetotail flux ropes are force-free (Amm et al., 2006; Henderson, Owen, Lahiff, et al., 2006; Slavin et al., 2003). Although considerable focus has been on the magnetic reconnection process, this analysis can be applied in other structures, for example to examine the

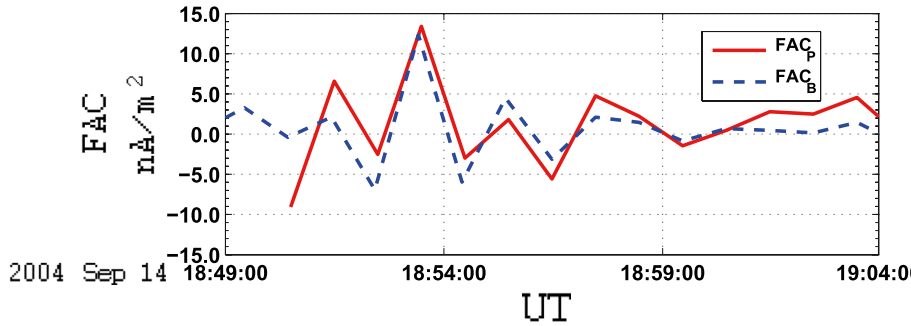

Figure 10. FAC densities, calculated by C3 ions and electron data (FAC_P) and the "curlometer" with the magnetic field data (FAC_B). Modified from Shi et al. (2010).

properties of plasma turbulence and the role of the various terms in the generalized Ohm's law at different scales (Stawarz et al., 2021).

Energy conversion between the particles and fields (E is the electric field, S is Poynting flux density and U is the electromagnetic field energy density) is controlled by the Joule term $\boldsymbol{E} \cdot \boldsymbol{j}$ where

$$-\boldsymbol{E} \cdot \boldsymbol{J} = \nabla \cdot \boldsymbol{S} + \frac{\partial U_{\text{field}}}{\partial t}$$

and an equivalent equation can be written for the particle energy density and energy flux (e.g., Goldman et al., 2016). Energy conversion regions are therefore marked at a basic level by this parameter; if $\boldsymbol{E} \cdot \boldsymbol{j} > 0$, then assuming energy fluxes are negligible, the field energy density is decreasing and this is referred to as a load region (i.e., energy is being passed from the fields to the particles. Conversely, if $\boldsymbol{E} \cdot \boldsymbol{j} < 0$ then under the same assumptions, the field energy density is increasing and energy is being passed from the particles to the fields in what is termed a generator region. The frame of reference is of particular importance and so a generalized frame independent measure of work has been suggested based on $\boldsymbol{j} \cdot \boldsymbol{E}'$ where $\boldsymbol{E}' = \boldsymbol{E} + \boldsymbol{u}_e \times \boldsymbol{B}$ (Zenitani et al., 2011).

Identification and analysis of energy conversion regions therefore fundamentally depends on the ability to calculate the current density accurately, as well as to assess the electric field. Pioneering work using the four-point Cluster measurements enabled the identification of so-called concentrated generator regions in the magnetotail, correlating with FAST satellite observations of auroral precipitation on connected field lines (Hamrin et al., 2006, 2009, 2011; Marghitu et al., 2006). In particular, Hamrin et al., 2006; apply the curlometer to identify generator regions (where $E.J < 0$) when Cluster was in the magnetotail plasma sheet near apogee on September 19, 2001, while FAST was magnetically conjugate. These regions of negative $\boldsymbol{E} \cdot \boldsymbol{j}$ provided novel insight into the role of magnetotail processes in creating auroral generator regions.

Subsequent analysis using Cluster found extensive evidence for both load ($\boldsymbol{E} \cdot \boldsymbol{J} > 0$) and generator regions in the magnetotail ($\boldsymbol{E} \cdot \boldsymbol{J} < 0$), with a tendency for more load regions than generator regions to be observed. This implies that the magnetotail is more generally a region where the plasma is energized at the expense of the fields (Hamrin et al., 2009; Hamrin et al., 2011). More specifically, Cluster multipoint curlometry revealed the creation of generator regions in the pile-up region associated with dipolarisation fronts at the leading edge of bursty bulk flows (Hamrin et al., 2013) and the way in which bursty bulk flows are braked as they propagate Earthward (Hamrin et al., 2014). More recent work using curlometry to assess the current density, and also using MMS (where comparison with current density derived from the plasma measurements is also possible), has shown that the dipolarisation front is indeed an important location for the conversion and dissipation of energy (Zhong et al., 2019). More generally, $\boldsymbol{j} \cdot \boldsymbol{E}$ has been an important component of multiple studies using MMS to assess magnetotail reconnection energization (Torbert et al., 2016, 2018).

Energy conversion at the magnetopause has received similar attention, including using Cluster and curlometry techniques to calculate the current density (Anekallu et al., 2011). With the launch of MMS, curlometry to calculate the current density has played an important role in the study of magnetopause reconnection (e.g.,

Burch, Torbert, et al., 2016) and calculation of energy transport (e.g., Genestreti et al., 2018). Most recently, the first direct measurement of the dissipation rate spectrum in space plasma turbulence has been proposed by He et al. (2019). The dissipation rate around ion scales is found to exhibit a positive bulge in an ion cyclotron wave event, hence demonstrating the localized dissipation process occurring in the turbulent medium. The curlometer method is also used to estimate the current for computing the energy cascade rate in Andres et al. (2019) and Bandyopadhyay et al. (2020).

4.7. Magnetic Reconnection and FTE's

Magnetic reconnection is a key plasma process in astrophysical, solar, space, and laboratory plasmas, through which energy stored in the magnetic field is explosively released and converted (in the reconnection current sheet) to the charged particles. Current structures in the reconnection region have been revealed by the curlometer, using the in-situ data of Cluster and MMS, which also has identified the Hall current system in the ion diffusion region directly (e.g., Zhou et al., 2009, 2011; and see also Section 4.6) and indeed important evidence from MMS identifying the electron diffusion region for a strong thin current sheet and its associated large energy dissipation rate $\boldsymbol{j} \cdot \boldsymbol{E}'$ has been shown (Zenitani et al., 2011). Many reconnection electron diffusion events have been reported in different regions of the magnetosphere (e.g., André et al., 2016; Burch, Torbert et al., 2016; Dong et al., 2020; Ergun et al., 2018; Hwang et al., 2019; Nakamura et al., 2019; Øieroset et al., 2016; Peng et al., 2017; Vörös et al., 2017; Wang et al., 2017; Yordanova et al., 2016; Zhou et al., 2016). Furthermore, the current surrounding the turbulent magnetic reconnection region can exhibit filamentary structures and the energy dissipation associated with them has been shown to be important (Fu et al., 2017).

Flux transfer events (FTEs) are transient signatures from the passage of magnetic flux ropes formed by magnetic reconnection at the MP, which are typically characterized by a bipolar magnetic field signature in the normal component to the magnetopause (Russell & Elphic, 1979) and contain a mixture of magnetosheath-like and magnetospheric-like plasmas (Paschmann et al., 1982). The force-free flux rope model is widely used to fit the observational signatures, in which the magnetic pressure force is balanced by the magnetic curvature force; although an excellent fit to the force-free flux rope model does not necessarily prove the actual existence of such a flux rope (Hasegawa et al., 2007). Using the curlometer, the force-free feature can be identified unambiguously by checking the ratio of perpendicular and parallel current. FTEs were found to be either force-free ($\boldsymbol{J} \times \boldsymbol{B} = 0$) structure or not (Farrugia et al., 2016; Roux et al., 2015; Teh et al., 2017). Using the force analysis by four spacecraft, Zhao et al. (2016) found that the plasma force, and especially the ion pressure force, must be considered when the FTE is not force-free. The detailed current structure inside FTEs is also a problem which has been considered. Robert et al., 2002; revealed a double-current structure (and see below, Roux et al., 2015), with the current antiparallel to the magnetic field in the outer region of the FTE, but parallel around the central region (see also: Pu et al., 2005, 2007; De Keyser et al., 2005; Xiao et al., 2004; Zuo et al., 2004). In addition to FTEs, the curlometer is also widely used to analysis other flux ropes and flux rope-like structures (e.g., plasmoid, magnetic island) in other magnetospheric regions (Henderson, Owen, Alexeev, et al., 2006; Yao et al., 2020).

An FTE observed early in the Cluster mission is shown in Figure 11 (after Roux et al., 2015), showing a slightly complex bipolar signature, where $|B|$ increases twofold. The spacecraft encounters the leading region of the FTE at this peak in $|B|$, where the potential (a proxy for the density, panel g) decreases, as determined from EFW (Gustafsson et al., 1997). In the trailing region (region C) this density (potential), is similar to that in the magnetosheath (in regions A and D, before and after the event) and consists of two, brief, large rotations toward the magnetic field.. A dynamical spectrum of magnetic fluctuations (panel f) is strongly enhanced during the FTE. The different regions (D1, D2, D3) are marked by yellow vertical regions bracketed by pink lines, where the magnetic field undergoes sharp discontinuities at D2 and D3, where there are also rapid jumps in B_L. The measured magnetic field compares well to the Tsyganenko field in region C, suggesting first the inward (D2) and later outward (D3) boundaries are crossed. This is consistent with a density dip (between D2 and D3).

The size of the FTE is of order 1 R_E, larger than the size of the (regular) configuration, so we expect the curlometer to be accurate (Dunlop et al., 1988; Robert et al., 1998). The current density is plotted in panel e (using the formulism of Chanteur; Harvey, 1998a, 1998b). A relatively large current density exists during region B ($J_{max} \sim 25\ nA/m^2$) and lies approximately along the azimuthal direction and nearly antiparallel to B (toward the evening sector). This suggests that the MFLs are twisted strongly. It is found that the main magnetic field component in region B is associated with the current where B_L is antiparallel to the expected direction. This interpretation

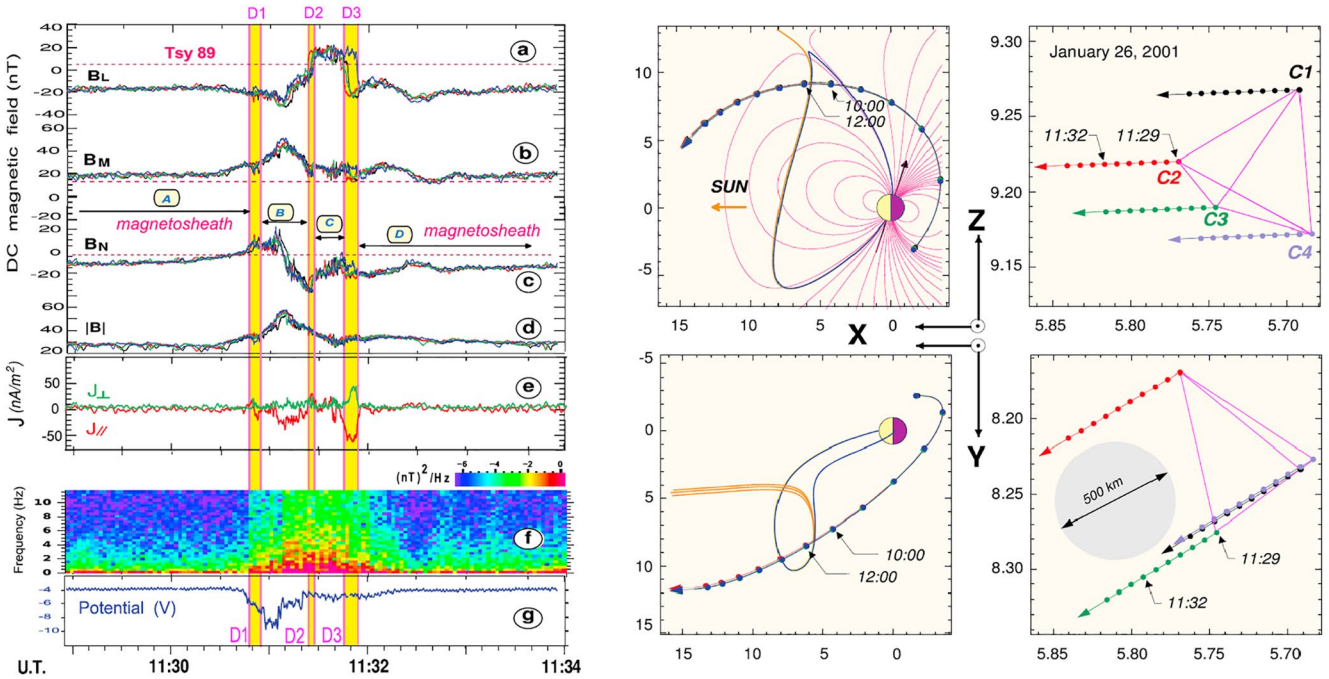

Figure 11. (left panel) The event of January 26, 2001, showing: full-cadence magnetic field (a–d) in L, M, N coordinates in *nT*. (e) *J* in nA/m^2, (f) the magnetic power spectral density in (nT)2/Hz, and (g) spacecraft potential in volts. (middle panels) (top) The Cluster orbit in GSE coordinates (magnetic field lines (MFL) are indicated, deduced from the Tsyganenko 89 model), projected into X, Z. (bottom) Cluster orbit in X, Y showing the location in the afternoon sector; near 11:30 UT. (right columns) The Cluster tetrahedron, projected into X, Z and X, Y, also in GSE. The spacecraft separation distance is 500–600 km. The Figure is adapted from Roux et al. (2015).

suggests that B_L can be similar to the magnetosheath field and also negative on closed field lines. The core of the flux rope corresponds to the leading region of the FTE (region B).

5. Recent Applications to MMS Configuration Scales

In principle, plasma currents can of course be obtained from the bulk moments of the measured, full 3D distribution of particle velocity for all ion species and electrons, although previous space missions have been limited to low cadence (since the distribution is taken over a spacecraft spin) or else the particle measurements are incomplete (the use of particle moments previously can be found in Henderson et al. (2008); Petrukovich, (2015), and indeed Yao et al. (2014), who also compared magnetic field derived currents to pressure gradients using multi-spacecraft techniques). The Magnetospheric Multiscale (MMS) mission, however, benefits from plasma distributions measured at high-time resolution (covering primarily the outer magnetosphere), in addition to the multi-point sampling at small (several km) spatial distances. Whereas the Cluster configuration was usually of the order or greater than the MPBL, particularly for the thin boundary layers, the MMS configuration is generally much smaller than the prevailing ion structure. In fact, it is generally true that in many regions of the magnetosphere there are intense small scale currents which are missed on the separation scales of Cluster (100s km) so that typically the curlometer tends to underestimate the current density, unless the current layers are much larger than the separation. Conversely, the current layers will often be much larger than the MMS separation scales so that ion-scale structures can be resolved (for example, in the magnetopause boundary layer, the tail current sheet, the ring current, or for field-aligned currents (FACs) and large scale flux tubes).

A number of papers have now studied currents using MMS plasma moments (e.g., Lavraud et al., 2016; Phan et al., 2016). Using MMS data, details of the sub-structure (Section 5.1) and smaller sub-proton to electron scale current layers and their detailed current carriers can be analyzed for the first time (Section 5.2). Conjunctions of Cluster and MMS provide the opportunity to compare the multiple scales of the magnetopause current system and simultaneous crossings at different locations on the MP current layer observed by Cluster can be compared (Section 5.3).

5.1. Sub-Structure in the MP and FTEs

The left hand side of Figure 12 shows the curlometer application to MMS data at the magnetopause (after Dunlop et al., 2018) in comparison to the current estimated from the plasma moments ($J = \sum qn_s V_s \sim qn\,(V_i - V_e)$), which closely follow the curlometer when averaged over the four spacecraft positions (the field perpendicular (Chapman-Ferraro current) and parallel (field-aligned current) components and the component normal to the MP, are shown separately). The normal component shows the most significant differences between the plasma currents and the curlometer. Panel (e) shows that for currents below ~50 nAm^{-2} both error sources are significant. The plasma current estimated at each spacecraft (bottom panel) varies significantly, however, implying that small scale (filamentary) structure within the magnetopause layer exists and that the dominant current carriers are measured by the plasma moments. Such small-scale structure is consistent with the intense, narrow bursts of current in the curlometer profile and appears to be typical of the magnetopause layer (Dong et al., 2018). Such substructure was not well resolved by Cluster (except for the smallest separation scales): the Cluster array trends to underestimate the current density and miss the filamentary currents.

Recently, many other researchers have focused on the structure of ion-scale FTEs, due to the improved time resolution of plasma data and small separation between four spacecraft (e.g., Alm et al., 2018; Dong et al., 2017, 2020; Eastwood et al., 2016; Hwang et al., 2018; Teh et al., 2017; Zhao et al., 2016). The first current structure in ion-scale FTEs, calculated by consistent results between the curlometer and plasma moments was shown by Eastwood et al. (2016), where electrons were the main current carriers, and filamentary currents were found within the FTEs. The right-hand side of Figure 12 shows two ion-scale FTEs and their detailed current structures (Dong et al., 2017). We see the currents are highly inhomogeneous and mainly located in the centre and on the leading edge of FTE. Furthermore, the current in the centre show bifurcated features. Parallel currents are dominate for most of time, which means they are force-free structures.

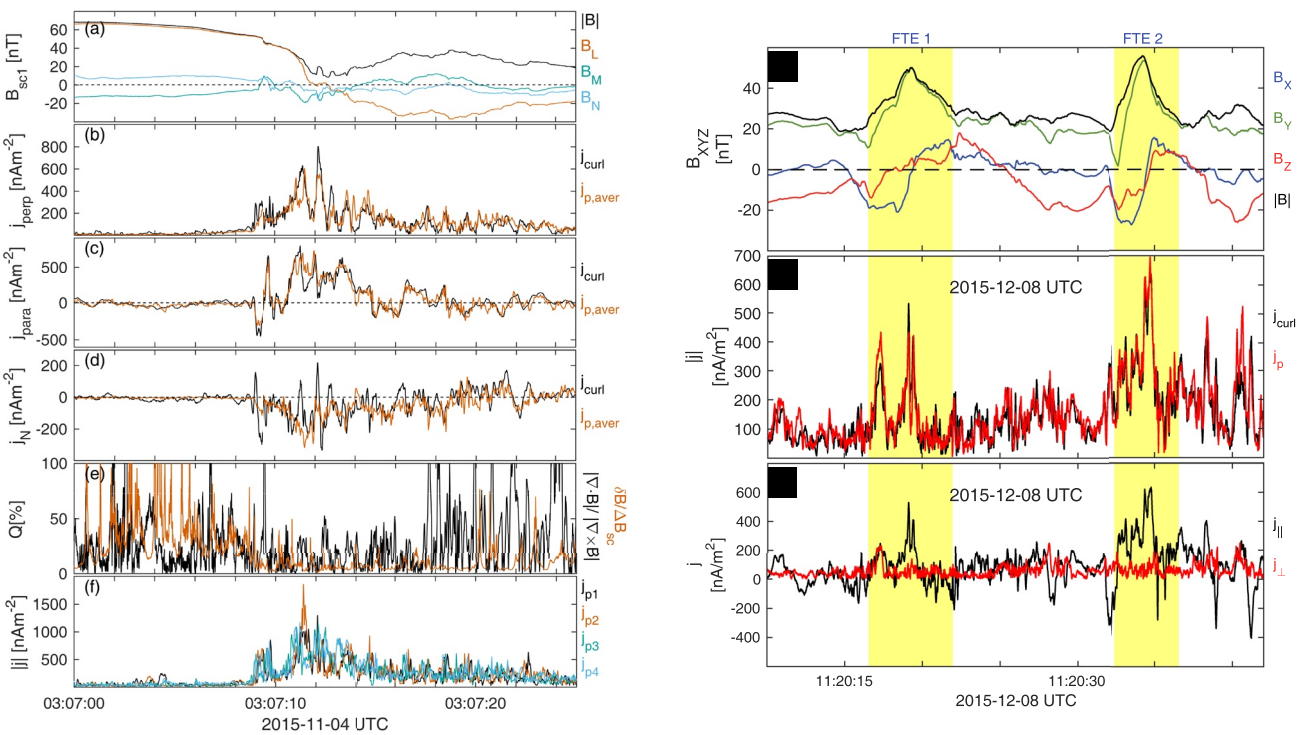

Figure 12. (left) A typical MP crossing for a thickness of ~350 km seen by MMS, showing: (a) L, M, N coordinates of the magnetic field, (b) to (d) the perpendicular, parallel and normal components of J from the curlometer estimate and the mean value of the 4-spacecraft ion moments, (e) the quality parameter Q compared to a crude (upper) estimate of the measurement errors from δB/ΔB, (f) the individual $|J|$ from the plasma moments at each spacecraft. (right) Detailed current structures of two ion-scale FTEs: (a) magnetic field with bipolar signatures in the normal component (B_x) during each FTE interval; (b) A consistent current result from the curlometer and plasma moments, respectively, and (c) Parallel and perpendicular currents (after Dong et al., 2017).

5.2. Carriers and Sources of Magnetopause Current

Figure 13 shows a thin MP current layer (~100 km) event encountered by MMS, which was studied by Dong et al. (2018). During this MP current layer, ions and electrons contribute comparable perpendicular current, while electrons contribute all the parallel current. For the perpendicular currents, the diamagnetic current term ($\boldsymbol{J}_{\rm dia} = \frac{B \times \nabla p_{\perp}}{B^2}$) and the directly measured $J_{\perp}$ shows good agreement (red line in Figures 2b and 2c) while the curvature current $\boldsymbol{J}_{{\rm dia},c} = -\frac{p_{\parallel} - p_{\perp}}{B^2 R_c}\boldsymbol{B} \times \boldsymbol{n}$ can be neglected (green line in Figures 2b and 2c). When the diamagnetic current is separated into ion and electron components, the perpendicular current is dominated by the ion diamagnetic current ($J_{i,\rm dia}$: 85%, $J_{e,\rm dia}$: 15%, Figures 2d and 2e). Under the redistribution of the electric field, ions and electrons ultimately carry comparable current. The schematic on the bottom of Figure 2 shows all the vectors

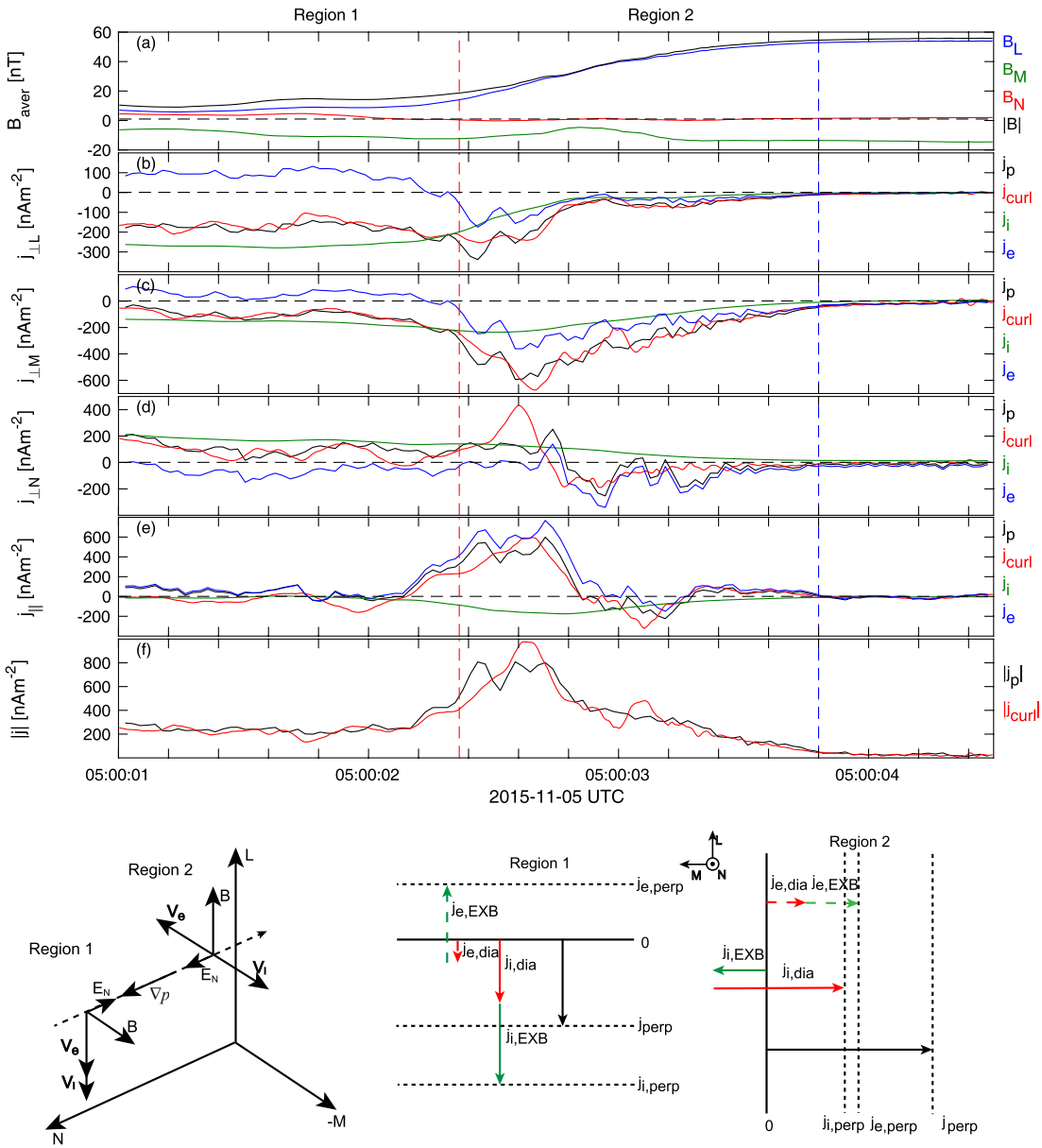

Figure 13. Top: Sources of a thin magnetopause current sheet calculated by MMS data. Bottom part: a schematic illustrator of all the vectors. (left) The vectors of magnetic field B, electric field E, plasma velocity V, cross-field drift $E \times B$, and gradient of pressure ∇p in regions 1 and 2 and (middle and right) current distribution in region 1 and region 2. Note that region 1 and 2 here refer to the outer and inner magnetopause current sheet region, respectively. The Figure is adopted from Dong et al. (2018).

in regions 1 and 2. Furthermore, electron current deviates at a narrow front layer in region 2 which suggests non-MHD behavior (beyond Chapman-Ferraro).

5.3. Current Observed by Simultaneous MMS and Cluster Magnetopause Crossings

Figure 14 shows an MMS magnetopause current layer crossing compared with an almost simultaneous crossing at different locations observed by Cluster. The crossing of MMS is located near the subsolar region and Cluster is located on the high latitude post-noon region (Figure 14n–o). The crossing time of MMS is only ∼20 s later than Cluster. The average separation of four MMS spacecraft is ∼8 km which is much smaller than the current layer thickness ∼440 km while the four Cluster spacecraft is ∼3,500 km which is large compared to the current layer thickness of ∼1,400 km. Therefore, the detailed structure of small-scale current can be revealed quantitatively by MMS, while the overall current can be underestimated by Cluster. Indeed, the average current of MMS during the shaded region (Figure 3e) is about 220 nA/m^{-2} which is one order larger than Cluster results (Figure 14m).

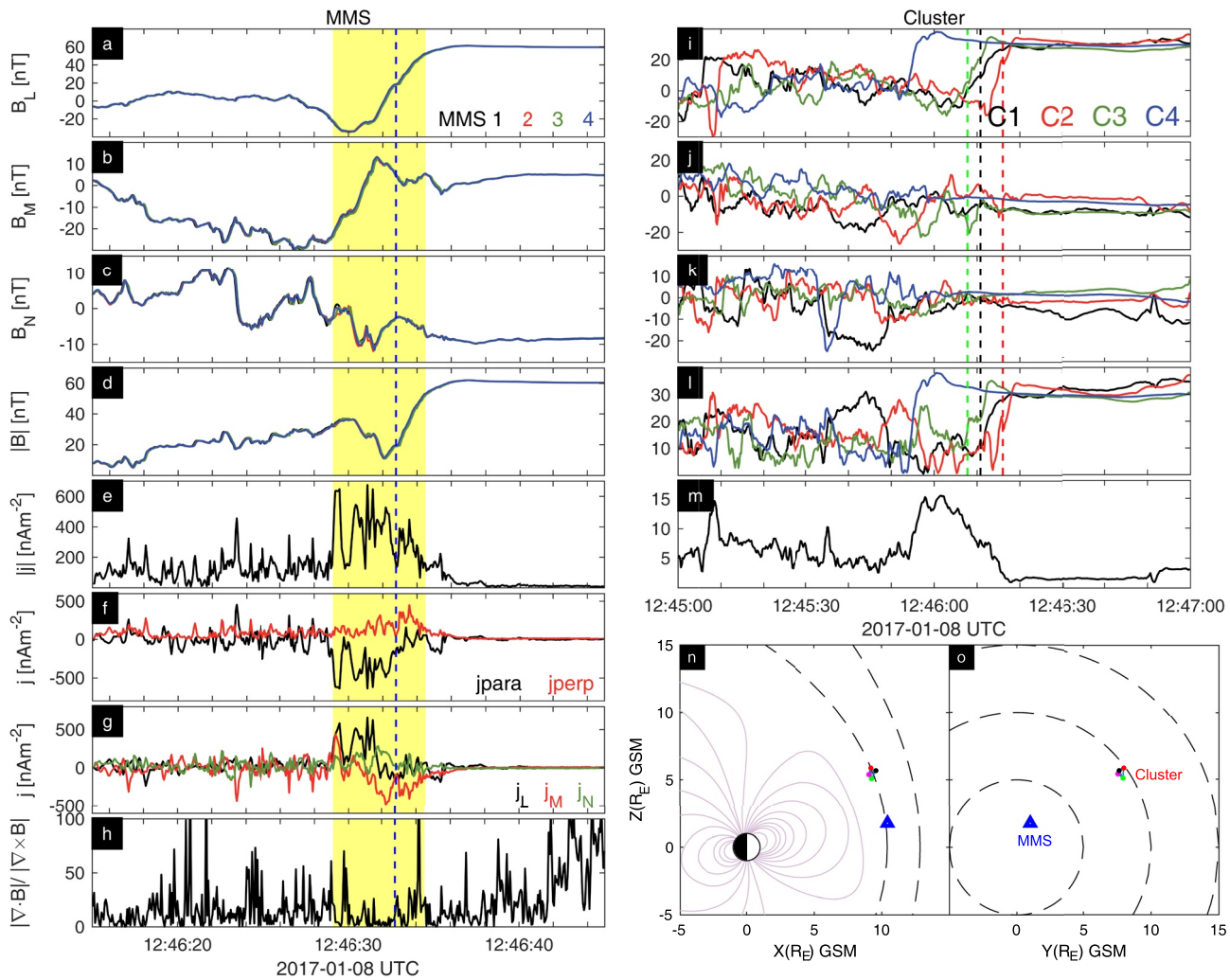

Figure 14. Magnetic field and current observed by a simultaneous MMS (left) and Cluster (right) magnetopause crossing. (a–d and i–l)Vector magnetic field in GSM coordinate. (e and m) Electric current from curlometer method. (f) MMS current in parallel and perpendicular direction, respectively. (g) MMS current in local boundary normal coordinate. (n–o) Magnetopause crossings locations of MMS [(10.4, 1.0, 1.8) R_E] and Cluster [(9.6, 7.6, 5.7) R_E] at XZ and YZ plane, respectively.

Table 2
Simultaneous MMS and Cluster MP Crossing Events With Delta Time <30 s During 2017–2018

Event	MMS date and time (UTC)	MMS position (GSM, R_E)	Cluster date and time (UTC)	Cluster position (GSM)
1	2017-01-08 12:46:32	(10.4, 1.0, 1.8)	2017-01-08 12:46:10	(9.6, 7.6, 5.7)
2	2017-01-29 00:55:45	(8.4, −6.5, −2.5)	2017-01-29 00:55:05	(8.1, −1.9, 7.7)
3	2017-02-07 01:06:40	(8.02, −7.5, −2.9)	2017-02-07 01:06:40	(9.4, −3.2, 6.6)
4	2018-01-12 05:46:00	(11.2, 5.1, 4.8)	2018-01-12 05:46:10	(8.6, 3.7, 8.7)

From the results of MMS, we see the current along the parallel direction (j_{para}) is dominant during magnetosheath side current sheet and extended to magnetosheath region where magnetic field component B_L contra-rotation to a negative value (Figures 14a and 14f This kind of B_L feature is also observed by four spacecraft of Cluster (Figure 14i) which indicates a similar current structure between MMS and Cluster. The current sheet of MMS shows a bifurcated structure divided by a small current region which is noted by the vertical dashed line on the left side. This small current region corresponding to a flat structure of B_L (Figure 14a). This kind of B_L feature is also similar to Cluster 1,2 and 3 which are noted by the vertical dashed line on the right side (Figure 14i). It indicates that the bifurcated current structure also exists during the region of Cluster. However, this feature is not observed by Cluster 4 when it crossed ∼15 s before which may suggest that this kind of current sheet is highly dynamic on a time scale.

We list all the simultaneous MMS and Cluster magnetopause crossing events with delta time <30 s during years 2017–2018 in Table 2. A similar current structure between MMS and Cluster is further confirmed in Event 2 and Event 4. Above all, the magnetopause boundary layer sampled at two locations has a similar overall form for the magnetic field suggests that the MP should have a similar current structure across a wide region during specific IMF conditions. However, in another simultaneous event (Event 3) which was studied by Escoubet et al. (2020), the magnetopause current structures encountered by Cluster and MMS are totally different under the effect of the high-speed jet in the magnetosheath. This suggests that similar current structures across a wide region can only remain during relatively stable solar wind conditions.

Note that MMS also allows us, for the first time to compute the flow vorticity on basis of the curlometer approximation (Dunlop, Balogh, Glassmeier, et al., 2002; Dunlop, Balogh, Cargill et al., 2002), which also provides a linear gradient estimation for the velocity field (see Section 4.5). On the one hand, electron vorticities and their relation with electron currents have been studied in the turbulent magnetosheath (Chasapis et al., 2018; Phan et al., 2016), while on the other hand, the alignment of parallel ion vorticity and parallel current density are found to indicate the presence of coherent Alfvén vortex in the same region (Wang et al., 2019).

6. Summary

The multi-spacecraft estimates of current density point by point in time using the curlometer, from Cluster (and the adaptations to the SWARM and MMS missions later on) have provided a great deal of information about both large and small magnetospheric current systems and transient structures. The method has been able to determine 3D currents for a range of parameters in the widely different geospace regions; proving itself to be a tool which is reliable and robust. We have only been able to cover a limited set of applications and regions developed over the last two decades of closely spaced multipoint observations. Other applications have been covered elsewhere in this publication, however. The purpose here has been to show where key applications have been carried out. The applicability of the method is limited by certain constraints, particularly for structures that are small compared to the distances between the spacecraft, such as: the form of the spacecraft configuration and the presence of magnetic contributions from other (non-current) sources. Comparative estimates from particle moments, giving direct current density determination, can be used to add constraints in generalized methods computing magnetic gradients beyond linear order (Shen, Zhang, et al., 2021; Shen, Zhou, et al., 2021).

Data Availability Statement

The Swarm satellite data used in this study are available from ESA at http://swarm-diss.eo.esa.int/. For MMS data visit https://lasp.colorado.edu/mms/sdc/public/. Cluster data can be found at http://www.cosmos.esa.int/web/csa/.

Acknowledgments
MWD is supported by the NSFC grants 41821003, 41874193, and by NERC Highlight Topic SWIGS grant NE/P016863/1 and by STFC in-house research grant (ST/M001083/1). JE is supported by STFC ST/S000364/1.

References

Alexandrova, O. (2008). Solar wind vs. magnetosheath turbulence and Alfven vortices. *Nonlinear Processes in Geophysics*, *15*, 95–108. https://doi.org/10.5194/npg-15-95-2008

Alexandrova, O., Mangeney, A., Maksimovic, M., Cornilleau-Wehrlin, N., Bosqued, J.-M., & André, M. (2006). Alfvén vortex filaments observed in magnetosheath downstream of a quasi-perpendicular bow shock. *Journal of Geophysical Research*, *111*, A12208. https://doi.org/10.1029/2006JA011934

Alm, L., Farrugia, C. J., Paulson, K. W., Argall, M. R., Torbert, R. B., Burch, J. L., et al. (2018). Differing properties of two ion-scale magnetopause flux ropes. *Journal of Geophysical Research: Space Physics*, *123*(1), 114–131. https://doi.org/10.1002/2017JA024525

Amm, O., Donovan, E. F., Frey, H., Lester, M., Nakamura, R., Wild, J. A., et al. (2005). Coordinated studies of the geospace environment using cluster, satellite and ground-based data: An interim review. *Annales Geophysicae*, *23*, 2129–2170. https://doi.org/10.5194/angeo-23-2129-2005

Amm, O., Nakamura, R., Frey, H. U., Ogawa, Y., Kubyshkina, M., Balogh, A., & Reme, H. (2006). Substorm topology in the ionosphere and magnetosphere during a flux rope event in the magnetotail. *Annales Geophysicae*, *24*, 735–750. https://doi.org/10.5194/angeo-24-735-2006

André, M., Li, W., Toledo-Redondo, S., Khotyaintsev, Y. V., Vaivads, A., Graham, D. B., et al. (2016). Magnetic reconnection and modification of the Hall physics due to cold ions at the magnetopause. *Geophysical Research Letters*, *43*(13), 6705–6712. https://doi.org/10.1002/2016gl069665

Andres, N., Sahraoui, F., Galtier, S., Hadid, L. Z., Ferrand, R., & Huang, S. Y. (2019). Energy cascade rate measured in a collisionless space plasma with MMS data and compressible hall magnetohydrodynamic turbulence theory. *Physical Review Letters*, *123*, 245101. https://doi.org/10.1103/physrevlett.123.245101

Anekallu, C. R., Palmroth, M., Pulkkinen, T. I., Haaland, S. E., Lucek, E., & Dandouras, I. (2011). Energy conversion at the Earth's magnetopause using single and multispacecraft methods. *Journal of Geophysical Research*, *116*, A11204. https://doi.org/10.1029/2011JA016783

Angelopoulos, V. (2008). The THEMIS mission. *Space Science Reviews*, *141*, 5–34. https://doi.org/10.1007/s11214-008-9336-1

Artemyev, A. V., Angelopoulos, V., Halekas, J. S., Vinogradov, A. A., Vasko, I. Y., & Zelenyi, L. M. (2018). Dynamics of intense currents in the solar wind. *The Astrophysical Journal*, *859*(2), 95. https://doi.org/10.3847/1538-4357/aabe89

Artemyev, A. V., Petrukovich, A. A., Frank, A. G., Nakamura, R., & Zelenyi, L. M. (2013). Intense current sheets in the magnetotail: Peculiarities of electron physics. *Journal of Geophysical Research: Space Physics*, *118*(6), 2789–2799. https://doi.org/10.1002/jgra.50297

Artemyev, A. V., Petrukovich, A. A., Nakamura, R., & Zelenyi, L. M. (2015). Statistics of intense dawn-dusk currents in the Earth's magnetotail. *Journal of Geophysical Research: Space Physics*, *120*(5), 3804–3820. https://doi.org/10.1002/2015ja021046

Artemyev, A. V., Petrukovich, A. A., Zelenyi, L. M., Nakamura, R., Malova, H. V., & Popov, V. Y. (2009). Thin embedded current sheets: Cluster observations of ion kinetic structure and analytical models. *Annales Geophysicae*, *27*, 4075–4087. https://doi.org/10.5194/angeo-27-4075-2009

Artemyev, A. V., Pritchett, P. L., Angelopoulos, V., Zhang, X.-J., Nakamura, R., Lu, S., et al. (2018). Field-aligned currents originating from the magnetic reconnection region: Conjugate MMS-ARTEMIS observations. *Geophysical Research Letters*, *45*, 5836–5844. https://doi.org/10.1029/2018gl078206

Bandyopadhyay, R., Sorriso-Valvo, L., Chasapis, A., Hellinger, P., Matthaeus, W. H., Verdini, A., et al. (2020). In situ observation of hall magnetohydrodynamic cascade in space plasma. *Physical Review Letters*, *124*, 225101. https://doi.org/10.1103/physrevlett.124.225101

Berchem, J., & Russell, C. T. (1982). The thickness of the magnetopause current layer: ISEE 1 and 2 observations. *Journal of Geophysical Research*, *87*(A4), 2108–2114. https://doi.org/10.1029/JA087iA04p02108

Burch, J. L., Moore, T. E., Torbert, R. B., & Giles, B. L. (2016). Magnetospheric multiscale overview and science objectives. *Space Science Reviews*, *5*, 1–17. https://doi.org/10.1007/s11214-015-0164-9

Burch, J. L., Torbert, R. B., Phan, T. D., Chen, L.-J., Moore, T. E., Ergun, R. E., et al. (2016). Electron-scale measurements of magnetic reconnection in space. *Science*, *352*, aaf2939. https://doi.org/10.1126/science.aaf2939

Cao, J.-B., Yan, C., Dunlop, M., Reme, H., Dandouras, I., Zhang, T., et al. (2010). Geomagnetic signatures of current wedge produced by fast flows in a plasma sheet. *Journal of Geophysical Research*, *115*, A08205. https://doi.org/10.1029/2009JA014891

Chanteur, G. (1998). Spatial interpolation for four spacecraft: Theory. In *`Analysis methods for multispacecraft data', ISSI science report. SR-001* (pp. 395–418). Kluwer Academic Pub.

Chasapis, A., Retinò, A., Sahraoui, F., Vaivads, A., Khotyaintsev, Y. V., Sundkvist, D., et al. (2015). Thin current sheets and associated electron heating in turbulent space plasma. *The Astrophysical Journal Letters*, *804*(1), L1. https://doi.org/10.1088/2041-8205/804/1/l1

Chasapis, A., Yang, Y., Matthaeus, W. H., Parashar, T. N., Haggerty, C. C., Burch, J. L., et al. (2018). Energy conversion and collisionless plasma dissipation channels in the turbulent magnetosheath observed by the Magnetospheric Multiscale mission. *The Astrophysical Journal*, *862*, 32. https://doi.org/10.3847/1538-4357/aac775

Chen, Y., Zhang, T., Wu, M., Wang, G., Schmid, D., Baumjohann, W., et al. (2019). Small spatial-scale field-aligned currents in the plasma sheet boundary layer surveyed by magnetosphere multiscale spacecraft. *Journal of Geophysical Research: Space Physics*, *124*, 9976–9985. https://doi.org/10.1029/2019JA027027

Chen, Y. Q., Wu, M., Zhang, T. L., Huang, Y., Wang, G. Q., Nakamura, R., et al. (2021). Statistical characteristics of field-aligned currents in the plasma sheet boundary layer. *Journal of Geophysical Research: Space Physics*, *126*(2). https://doi.org/10.1029/2020JA028319

Cheng, Z.-W., Shi, J.-K., Zhang, T.-L., & Liu, Z.-X. (2007). Probability of field-aligned currents observed by the satellite cluster in the magnetotail. *Chinese Physics Letter*, *24*, 1125–1127. https://doi.org/10.1088/0256-307X/24/4/076

Cheng, Z. W., Zhang, J. C., Shi, J. K., Kistler, L. M., Dunlop, M., Dandouras, I., et al. (2016). The particle carriers of field-aligned currents in the Earth's magnetotail during a substorm. *Journal of Geophysical Research A: Space Physics*, *121*(4), 3058–3068. https://doi.org/10.1002/2015JA022071

Dai, L., Wygant, J. R., Cattell, C. A., Thaller, S., Kersten, K., Breneman, A., et al. (2014). Cluster observations of fast magnetosonic waves in the heliosphere current sheet. *Geophysical Research Letters*, *41*(5), 1398–1405. https://doi.org/10.1002/2014gl059223

Dandouras, I., Rochel-Grimald, S., Vallat, C., & Dunlop, M. (2018). Terrestrial ring current: A review of cluster results based on the curlometer. In A. Keiling, O. Marghitu, & M. Wheatland (Eds.), *Electric currents in geospace and beyond* (pp. 115–126): John Wiley & Sons, Inc., AGU books. https://doi.org/10.1002/9781119324522.ch7

Darrouzet, F., De Keyser, J., Décréau, P. M. E., Lemaire, J. F., & Dunlop, M. (2006). Spatial gradients in the plasmasphere from Cluster. *Geophysical Research Letters*, *33*, L08105. https://doi.org/10.1029/2006GL025727

Davey, E. A., Lester, M., Milan, S. E., Fear, R. C., & Forsyth, C. (2012). The orientation and current density of the magnetotail current sheet: A statistical study of the effect of geomagnetic conditions. *Journal of Geophysical Research*, *117*. https://doi.org/10.1029/2012ja017715

De Keyser, J. (2008). Least-squares multi-spacecraft gradient calculation with automatic error estimation. *Annales Geophysicae*, *26*, 3295–3316. https://doi.org/10.5194/angeo-26-3295-2008

De Keyser, J., Darrouzet, F., Dunlop, M. W., & Décréau, P. M. E. (2007). Least-squares gradient calculation from multi-point observations of scalar and vector fields: Methodology and applications with Cluster in the plasmasphere. *Annales Geophysicae*, *25*, 971–987. https://doi.org/10.5194/angeo-25-971-2007

De Keyser, J., Dunlop, M. W., Owen, C. J., Sonnerup, B. U. Ö., Haaland, S. E., Vaivads, A., et al. (2005). Magnetopause and boundary layer. *Space Science Reviews*, *118*(1–4), 231–320. https://doi.org/10.1007/s11214-005-3834-1

Dong, X.-C., Dunlop, M. W., Trattner, K. J., Phan, T. D., Fu, H.-S., Cao, J.-B., et al. (2017). Structure and evolution of flux transfer events near dayside magnetic reconnection dissipation region: MMS observations. *Geophysical Research Letters*, *44*(12), 5951–5959. https://doi.org/10.1002/2017GL073411

Dong, X.-C., Dunlop, M. W., Wang, T.-Y., Cao, J.-B., Trattner, K. J., Bamford, R., et al. (2018). Carriers and sources of magnetopause current: MMS case study. *Journal of Geophysical Research: Space Physics*, *123*, 5464–5475. https://doi.org/10.1029/2018JA025292

Dong, X.-C., Dunlop, M. W., Wang, T.-Y., Trattner, K. J., Russell, C. T., & Giles, B. (2020). MMS observation of secondary magnetic reconnection beside ion-scale flux rope at the magnetopause. *Geophysical Research Letters*, *47*(16). https://doi.org/10.1029/2020GL089075

Dunlop, M. W., & Balogh, A. (2005). Magnetopause current as seen by Cluster. *Annales Geophysicae*, *23*(3), 901–907. https://doi.org/10.5194/angeo-23-901-2005

Dunlop, M. W., Balogh, A., Cargill, P., Elphic, R. C., Fornacon, K.-H., Georgescu, E., et al. (2002). Cluster observes the Earth's magnetopause: Coordinated four-point magnetic field measurements. *Annales Geophysicae*, *19*(10), 1449–1460.

Dunlop, M. W., Balogh, A., Glassmeier, K.-H., & Robert, P. (2002). Four-point Cluster application of magnetic field analysis tools: The Curlometer. *Journal of Geophysical Research*, *107*(A11), 1384. https://doi.org/10.1029/2001JA005088

Dunlop, M. W., & Eastwood, J. P. (2008). The Curlometer and other gradient based methods. In G. Paschmann, & P. W. Daly (Eds.), *Multi-spacecraft analysis methods revisited. ISSI science report, SR-008* (pp. 17–21). Kluwer Academic Pub.

Dunlop, M. W., Haaland, S., Dong, X.-C., Middleton, H., Escoubet, P., Yang, Y.-Y., et al. (2018). Multi-point analysis of current structures and applications: Curlometer technique. In A. Keiling, O. Marghitu, & M. Wheatland (Eds.), *Electric currents in geospace and beyond* (pp. 67–80). John Wiley & Sons, Inc., AGU books. https://doi.org/10.1002/9781119324522.ch4

Dunlop, M. W., Lavraud, B., Cargill, P., Taylor, M. G. G. T., Balogh, A., Réme, H., et al. (2005). Cluster observations of the cusp: Magnetic structure and dynamics. *Surveys in Geophysics*, *26*(1–3), 5–55. https://doi.org/10.1007/s10712-005-1871-7

Dunlop, M. W. & Luehr, H. (Eds.), (2020). *Ionospheric multi-satellite analysis tools: Approaches for deriving ionospheric parameters, ISSI scientific reports* (Vol. 17). Springer. https://doi.org/10.1007/978-3-030-26732-2

Dunlop, M. W., Southwood, D. J., Glassmeier, K.-H., & Neubauer, F. M. (1988). Analysis of multipoint magnetometer data. *Advances in Space Research*, *8*, 273–277. https://doi.org/10.1016/0273-1177(88)90141-X

Dunlop, M. W., Wang, T.-Y., Dong, X.-C., Fu, H.-S., Haarland, S., Shi, Q.-Q., et al. (2021). *Review of magnetic field-based multi-spacecraft techniques in the magnetosphere*. AGU books. https://doi.org/10.1002/9781119815624

Dunlop, M. W., & Woodward, T. I. (1998). `Discontinuity analysis: Orientation and motion. In *`Analysis methods for multispacecraft data', ISSI science report, SR-001*. Kluwer Academic Pub.

Dunlop, M. W., Yang, J.-Y., Yang, Y.-Y., Xiong, C., Lühr, H., Bogdanova, Y. V., et al. (2015). Simultaneous field-aligned currents at Swarm and Cluster satellites. *Geophysical Research Letters*, *42*, 3683–3691. https://doi.org/10.1002/2015GL063738

Dunlop, M. W., Yang, Y.-Y., Yang, J.-Y., Lühr, H., Shen, C., Olsen, N., et al. (2015). Multi-spacecraft current estimates at Swarm. *Journal of Geophysical Research*, *120*, 8307–8316. https://doi.org/10.1002/2015JA021707

Dunlop, M. W. J.-Y. Y., Yang, J.-Y., Yang, Y.-Y., (2020). Multi-spacecraft current estimates at Swarm. In M. W. Dunlop, & H. Luehr (Eds.), *Ionospheric multi-satellite analysis tools. ISSI scientific reports* (Vol. 17, pp. 83–116). Springer. https://doi.org/10.1007/978-3-030-26732-2_5

Eastwood, J. P., Bale, S. D., Mozer, F. S., & Hull, A. J. (2007). Contributions to the cross shock electric field at a quasiperpendicular collisionless shock. *Geophysical Research Letters*, *34*, L17104. https://doi.org/10.1029/2007gl030610

Eastwood, J. P., Balogh, A., Dunlop, M. W., & Smith, C. W. (2002). Cluster observations of the heliospheric current sheet and an associated magnetic flux rope and comparisons with ACE. *Journal of Geophysical Research*, *107*(A11), 1365. https://doi.org/10.1029/2001JA009158

Eastwood, J. P., Phan, T. D., Cassak, P. A., Gershman, D. J., Haggerty, C., Malakit, K., et al. (2016). Ion-scale secondary flux ropes generated by magnetopause reconnection as resolved by MMS. *Geophysical Research Letters*, *43*(10), 4716–4724. https://doi.org/10.1002/2016GL068747

Ergun, R. E., Goodrich, K. A., Wilder, F. D., Ahmadi, N., Holmes, J. C., Eriksson, S., et al. (2018). Magnetic reconnection, turbulence, and particle acceleration: Observations in the Earth's magnetotail. *Geophysical Research Letters*, *45*(8), 3338–3347. https://doi.org/10.1002/2018gl076993

Escoubet, C. P., Fehringer, M., & Goldstein, M. (2001). Introduction: The Cluster mission. *Annales Geophysicae*, *19*, 1197–1200. https://doi.org/10.5194/angeo-19-1197-2001

Escoubet, C. P., Hwang, K.-J., Toledo-Redondo, S., Turc, L., Haaland, S. E., Aunai, N., et al. (2020). Cluster and MMS simultaneous observations of Magnetosheath high speed jets and their impact on the Magnetopause. *Frontiers in Astronomy and Space Sciences*, *6*(January), 1–21. https://doi.org/10.3389/fspas.2019.00078

Farrugia, C. J., Lavraud, B., Torbert, R. B., Argall, M., Kacem, I., Yu, W., et al. (2016). Magnetospheric multiscale mission observations and non-force free modeling of a flux transfer event immersed in a super-Alfvénic flow. *Geophysical Research Letters*, *43*(12), 6070–6077. https://doi.org/10.1002/2016GL068758

Fillion, M., Hulot, G., Alken, P., Chulliat, A., & Vigneron, P. (2021). Multispacecraft current density estimates in the low- and midlatitude F-region ionosphere using the Swarm constellation. *Journal of Geophysical Research: Space Physics*, *126*. https://doi.org/10.1029/2020JA028872

Forsyth, C., Lester, M., Cowley, S. W. H., Dandouras, I., Fazakerley, A. N., Fear, R. C., et al. (2008). Observed tail current systems associated with bursty bulk flows and auroral streamers during a period of multiple substorms. *Annales Geophysicae*, *26*, 167–184. https://doi.org/10.5194/angeo-26-167-2008

Forsyth, C., Lester, M., Fazakerley, A., Owen, C., & Walsh, A. (2011). On the effect of line current width and relative position on the multi-spacecraft curlometer technique. *Planetary and Space Science*, *59*, 598–605. https://doi.org/10.1016/j.pss.2009.12.007

Friis-Christensen, E., Lühr, H., Knudsen, D., & Haagmans, R. (2008). Swarm – An earth observation mission investigating geospace. *Advances in Space Research*, *41*, 210–216. https://doi.org/10.1016/j.asr.2006.10.008

Fu, H. S., Cao, J., Vaivads, A., Khotyaintsev, Y. V., Andre, M., Dunlop, M., et al. (2016). Identifying magnetic reconnection events using the FOTE method. *Journal of Geophysical Research - A: Space Physics*, *121*, 1263–1272. https://doi.org/10.1002/2015ja021701

Fu, H. S., Khotyaintsev, Y. V., Vaivads, A., André, M., & Huang, S. Y. (2012). Electric structure of dipolarization front at sub-proton scale. *Geophysical Research Letters*, *39*(6). https://doi.org/10.1029/2012GL051274

Fu, H. S., Vaivads, A., Khotyaintsev, Y. V., André, M., Cao, J. B., Olshevsky, V., et al. (2017). Intermittent energy dissipation by turbulent reconnection. *Geophysical Research Letters*, *44*, 37–43. https://doi.org/10.1002/2016GL071787

Fu, H. S., Vaivads, A., Khotyaintsev, Y. V., Olshevsky, V., André, M., Cao, J., et al. (2015). How to find magnetic nulls and reconstruct field topology with MMS data? *Journal of Geophysical Research - A: Space Physics*, *120*, 3758–3782. https://doi.org/10.1002/2015ja021082

Genestreti, K. J., Cassak, P. A., Varsani, A., Burch, J. L., Nakamura, R., & Wang, S. (2018). Assessing the time dependence of reconnection with Poynting's theorem: MMS observations. *Geophysical Research Letters*, *45*, 2886–2892. https://doi.org/10.1002/2017GL076808

Gjerloev, J. W., & Hoffman, R. A. (2002). Currents in auroral substorms. *Journal of Geophysical Research*, *107*(A8), 5–1. https://doi.org/10.1029/2001JA000194

Goldman, M. V., Newman, D. L., & Lapenta, G. (2016). What can we learn about magnetotail reconnection from 2D PIC Harris-Sheet simulations? *Space Science Reviews*, *199*, 651–688. https://doi.org/10.1007/s11214-015-0154-y

Grimald, S., Dandouras, I., Robert, P., & Lucek, E. (2012). Study of the applicability of the curlometer technique with the four Cluster spacecraft in regions close to Earth. *Annales Geophysicae*, *30*, 597–611. https://doi.org/10.5194/angeo-30-597-2012

Gustafsson, G., Bostrom, R., Holback, B., Holmgren, G., Lundgren, A., Stasiewicz, K., et al. (1997). The electric field and wave experiment for the CLUSTER mission. *Space Science Reviews*, *79*(137). https://doi.org/10.1007/978-94-011-5666-0_6

Haaland, S., & Gjerloev, J. (2013). On the relation between asymmetries in the ring current and magnetopause current. *Journal of Geophysical Research*, *118*, 7593–7604. https://doi.org/10.1002/2013JA019345

Haaland, S., Reistad, J., Tenfjord, P., Gjerloev, J., Maes, L., DeKeyser, J., et al. (2014). Characteristics of the flank magnetopause: Cluster observations. *Journal of Geophysical Research*, *119*(11), 9019–9037. https://doi.org/10.1002/2014JA020539

Haaland, S., Sonnerup, B., Dunlop, M., Balogh, A., Georgescu, E., Hasegawa, H., et al. (2004). Four-spacecraft determination of magnetopause orientation, motion and thickness: Comparison with results from single-spacecraft methods. *Annales Geophysicae*, *22*(4), 1347–1365. https://doi.org/10.5194/angeo-22-1347-2004

Haaland, S., Sonnerup, B. Ö., Dunlop, M., Georgescu, E., Paschmann, G., Klecker, B., & Vaivads, A. (2004). Orientation and motion of a discontinuity from Cluster curlometer capability: Minimum variance of current density. *Geophysical Research Letters*, *31*, L10804. https://doi.org/10.1029/2004GL020001

Hamrin, M., Marghitu, O., Norqvist, P., Buchert, S., André, M., Klecker, B., et al. (2011). Energy conversion regions as observed by Cluster in the plasma sheet. *Journal of Geophysical Research: Space Physics*, *116*(A1). https://doi.org/10.1029/2010ja016383

Hamrin, M., Marghitu, O., Ronnmark, K., Klecker, B., Andre, M., Buchert, S., et al. (2006). Observations of concentrated generator regions in the nightside magnetosphere by cluster/fast conjunctions. *Annales Geophysicae*, *24*, 637–649. https://doi.org/10.5194/angeo-24-637-2006

Hamrin, M., Norqvist, P., Karlsson, T., Nilsson, H., Fu, H. S., Buchert, S., et al. (2013). The evolution of flux pileup regions in the plasma sheet: Cluster observations. *Journal of Geophysical Research: Space Physics*, *118*(10), 6279–6290. https://doi.org/10.1002/jgra.50603

Hamrin, M., Norqvist, P., Marghitu, O., Vaivads, A., Klecker, B., Kistler, L. M., et al. (2009). Scale size and life time of energy conversion regions observed by Cluster in the plasma sheet. *Annales Geophysicae*, *27*, 4147–4155. https://doi.org/10.5194/angeo-27-4147-2009

Hamrin, M., Pitkänen, T., Norqvist, P., Karlsson, T., Nilsson, H., André, M., et al. (2014). Evidence for the braking of flow bursts as they propagate toward the Earth. *Journal of Geophysical Research: Space Physics*, *119*(11), 9004–9018. https://doi.org/10.1002/2014ja020285

Hamrin, M., Rönnmark, K., Börlin, N., Vaivads, A., & Vaivads, A. (2008). GALS: Gradient analysis by least squares. *Annales Geophysicae*, *26*, 3491–3499. https://doi.org/10.5194/angeo-26-3491-2008

Harvey, C. C. (1998a). Spatial gradients and the volumetric tensor. In G. Paschmann, & P. W. Daly (Eds.), *Analysis methods for multi-spacecraft data. SR-001* (pp. 307–322). ISSI Scientific Report.

Harvey, C. C. (1998b). Spatial gradients and the volumetric tensor. In *`Analysis methods for multispacecraft data', ISSI science report, SR-001* (pp. 395–418). Kluwer Academic Pub.

Hasegawa, H., Nakamura, R., Fujimoto, M., Sergeev, V. A., Lucek, E. A., Rème, H., et al. (2007). Reconstruction of a bipolar magnetic signature in an earthward jet in the tail: Flux rope or 3D guide-field reconnection. *Journal of Geophysical Research*, *112*(11), 1. https://doi.org/10.1029/2007JA012492

Hau, L. N., Chen, G. W., & Chang, C. K. (2020). Mirror mode waves immersed in magnetic reconnection. *Astrophysical Journal Letters*, *903*, L12. https://doi.org/10.3847/2041-8213/abbf4a

He, J., Duan, D., Wang, T., Zhu, X., Li, W., Verscharen, D., et al. (2019). Direct measurement of the dissipation rate spectrum around ion kinetic scales in space plasma turbulence. *The Astrophysical Journal*, *880*(2), 121. https://doi.org/10.3847/1538-4357/ab2a79

Henderson, P. D., Owen, C. J., Alexeev, I. V., Slavin, J., Fazakerley, A. N., Lucek, E., et al. (2006). Cluster observations of flux rope structures in the near-tail. *Annales Geophysicae*, *24*, 651–666. https://doi.org/10.5194/angeo-24-651-2006

Henderson, P. D., Owen, C. J., Lahiff, A. D., Alexeev, I. V., Fazakerley, A. N., Lucek, E., et al. (2006). Cluster peace observations of electron pressure tensor divergence in the magnetotail. *Geophysical Research Letters*, *33*, L22106. https://doi.org/10.1029/2006GL027868

Henderson, P. D., Owen, C. J., Lahiff, A. D., Alexeev, I. V., Fazakerley, A. N., Yin, L., et al. (2008). The relationship between j and Pe in the magnetotail plasma sheet: Cluster observations. *Journal of Geophysical Research*, *113*, A07S31. https://doi.org/10.1029/2007JA012697

Huang, S. Y., Sahraoui, F., Retino, A., Le Contel, O., Yuan, Z. G., Chasapis, A., et al. (2016). MMS observations of ion-scale magnetic island in the magnetosheath turbulent plasma. *Geophysical Research Letters*, *43*(15), 7850–7858. https://doi.org/10.1002/2016gl070033

Hwang, K.-J., Choi, E., Dokgo, K., Burch, J. L., Sibeck, D. G., Giles, B. L., et al. (2019). Electron vorticity indicative of the electron diffusion region of magnetic reconnection. *Geophysical Research Letters*, *46*(12), 6287–6296. https://doi.org/10.1029/2019gl082710

Hwang, K.-J., Sibeck, D. G., Burch, J. L., Choi, E., Fear, R. C., Lavraud, B., et al. (2018). Small-Scale flux transfer events formed in the reconnection exhaust region between two X lines. *Journal of Geophysical Research: Space Physics*, *123*(10), 8473–8488. https://doi.org/10.1029/2018JA025611

Karlsson, T., Hamrin, M., Nilsson, H., Kullen, A., & Pitkänen, T. (2015). Magnetic forces associated with bursty bulk flows in Earth's magnetotail. *Geophysical Research Letters*, *42*(9), 3122–3128. https://doi.org/10.1002/2015GL063999

Khotyaintsev, Y., Vaivads, A., Ogawa, Y., Popielawska, B., André, M., Buchert, S., et al. (2004). Cluster observations of high-frequency waves in the exterior cusp. *Annales Geophysicae*, *22*, 2403–2411. https://doi.org/10.5194/angeo-22-2403-2004

Kivelson, M., & Russell, C. T. (1995). *Introduction to space physics*. Cambridge University Press.

Kivelson, M. G., McPherron, R. L., Thompson, S., Khurana, K. K., Weygand, J. M., & Balogh, A. (2005). The response of the near earth magnetotail to substorm activity. *Advances in Space Research*, *36*, 1818–1824. https://doi.org/10.1016/j.asr.2004.03.024

Laitinen, T. V., Nakamura, R., Runov, A., Reme, H., & Lucek, E. A. (2007). Global and local disturbances in the magnetotail during reconnection. *Annales Geophysicae*, *25*, 1025–1035. https://doi.org/10.5194/angeo-25-1025-2007

Lavraud, B., Zhang, Y. C., Vernisse, Y., Gershman, D. J., Dorelli, J., Cassak, P. A., et al. (2016). Currents and associated electron scattering and bouncing near the diffusion region at Earth's magnetopause. *Geophysical Research Letters*, *43*, 3042–3050. https://doi.org/10.1002/2016GL068359

Liang, J., & Liu, W. W. (2007). A MHD mechanism for the generation of the meridional current system during substorm expansion phase. *Journal of Geophysical Research*, *112*, A09208. https://doi.org/10.1029/2007JA012303

Liu, C. M., Fu, H. S., Xu, Y., Khotyaintsev, Y. V., Burch, J. L., Ergun, R. E., et al. (2018). Electron-scale measurements of dipolarization front. *Geophysical Research Letters*, *45*(10), 4628–4638. https://doi.org/10.1029/2018GL077928

Liu, J., Angelopoulos, V., Chu, X., Zhou, X., & Yue, C. (2015). Substorm current wedge composition by wedgelets. *Geophysical Research Letters*, *42*(6), 1669–1676. https://doi.org/10.1002/2015GL063289

Liu, J., Angelopoulos, V., Runov, A., & Zhou, X.-Z. (2013). On the current sheets surrounding dipolarizing flux bundles in the magnetotail: The case for wedgelets. *Journal of Geophysical Research: Space Physics*, *118*(5), 2000–2020. https://doi.org/10.1002/jgra.50092

Lühr, H., Park, J., Gjerloev, J. W., Rauberg, J., Michaelis, I., Merayo, J. M. G., et al. (2015). Field-aligned currents' scale analysis performed with the Swarm constellation. *Geophysical Research Letters*, *42*, 1–8. https://doi.org/10.1002/2014GL062453

Lui, A. T. Y., Zheng, Y., Reme, H., Dunlop, M. W., Gustafsson, G., & Owen, C. J. (2007). Breakdown of the frozen-in condition in the earth's magnetotail. *Journal of Geophysical Research*, *112*, A04215. https://doi.org/10.1029/2006JA012000

Marchaudon, A., Cerisier, J.-C., Dunlop, M. W., Pitout, F., Bosqued, J.-M., & Fazakerley, A. N. (2009). Shape, size, velocity and field-aligned currents of dayside plasma injections: A multi-altitude study. *Annales Geophysicae*, *27*, 1251–1266. https://doi.org/10.5194/angeo-27-1251-2009

Marghitu, O., Hamrin, M., Klecker, B., Vaivads, A., McFadden, J., Buchert, S., et al. (2006). Experimental investigation of auroral generator regions with conjugate cluster and fast data. *Annales Geophysicae*, *24*, 619–635. https://doi.org/10.5194/angeo-24-619-2006

Maynard, N. C., Burke, W. J., Scudder, J. D., Ober, D. M., Weimer, D. R., Siebert, K. D., et al. (2005). Electron signatures of active merging sites on the magnetopause. *Journal of Geophysical Research*, *110*, A10207. https://doi.org/10.1029/2004JA010639

Maynard, N. C., Farrugia, C. J., Burke, W. J., Ober, D. M., Mozer, F. S., Rème, H., et al. (2012). Cluster observations of the dusk flank magnetopause near the sash: Ion dynamics and flow-through reconnection. *Journal of Geophysical Research: Space Physics*, *117*(A10). https://doi.org/10.1029/2012JA017703

Maynard, N. C., Farrugia, C. J., Ober, D. M., Burke, W. J., Dunlop, M., Mozer, F. S., et al. (2008). Cluster observations of fast shocks in the magnetosheath launched as a tangential discontinuity with a pressure increase crossed the bow shock. *Journal of Geophysical Research*, *113*(10). https://doi.org/10.1029/2008JA013121

Maynard, N. C., Ober, D. M., Burke, W. J., Scudder, J. D., Lester, M., Dunlop, M., et al. (2003). Polar, Cluster and SuperDARN evidence for high-latitude merging during southward IMF: Temporal/spatial evolution, *Annales Geophysicae*, *21*, 2233–2258.

McPherron, R. L., Russell, C. T., & Aubry, M. P. (1973). Satellite studies of magnetospheric substorms on August 15, 1968: 9. Phenomenological model for substorms. *Journal of Geophysical Research*, *78*(16), 3131–3149. https://doi.org/10.1029/JA078i016p03131

Middleton, H. R., & Masson, A. (2016). *The curlometer technique: A beginner's guide*. ESA Technical Note ESDC-CSA_TN_0001. Retrieved from http://www.cosmos.esa.int/web/csa/multi-spacecraft

Nakamura, R., Baumjohann, W., Asano, Y., Runov, A., Balogh, A., Owen, C. J., et al. (2006). Dynamics of thin current sheets associated with magnetotail reconnection. *Journal of Geophysical Research*, *111*, A11206. https://doi.org/10.1029/2006JA011706

Nakamura, R., Baumjohann, W., Fujimoto, M., Asano, Y., Runov, A., Owen, C., et al. (2008). Cluster observations of an ion-scale current sheet in the magnetotail under the presence of a guide field. *Journal of Geophysical Research*, *113*. https://doi.org/10.1029/2007JA012760

Nakamura, R., Baumjohann, W., Klecker, B., Bogdanova, Y., Balogh, A., Rème, H., et al. (2002). Motion of the dipolarization front during a flow burst event observed by Cluster. *Geophysical Research Letters*, *29*(20), 3-1–3-4. https://doi.org/10.1029/2002GL015763

Nakamura, R., Baumjohann, W., Nagai, T., Fujimoto, M., Mukai, T., Klecker, B., et al. (2004). Flow shear near the boundary of the plasma sheet observed by Cluster and Geotail. *Journal of Geophysical Research*, *109*. https://doi.org/10.1029/2003JA010174

Nakamura, R., Genestreti, K. J., Nakamura, T., Baumjohann, W., Varsani, A., Nagai, T., et al. (2019). Structure of the current sheet in the 11 July 2017 electron diffusion region event. *Journal of Geophysical Research: Space Physics 124*, 1173–1186. https://doi.org/10.1029/2018JA026028

Nakamura, R., Varsani, A., Genestreti, K. J., Le Contel, O., Nakamura, T., Baumjohann, W., et al. (2018). Multiscalecurrents observed by MMS in the flow braking region. *Journal of Geophysical Research: Space Physics*, *123*, 1260–1278. https://doi.org/10.1002/2017ja024686

Narita, Y., Nakamura, R., & Baumjohann, W. (2013). Cluster as current sheet surveyor in the magnetotail. *Annales Geophysicae*, *31*, 1605–1610. https://doi.org/10.5194/angeo-31-1605-2013

Øieroset, M., Phan, T. D., Haggerty, C., Shay, M. A., Eastwood, J. P., Gershman, D. J., et al. (2016). MMS observations of large guide field symmetric reconnection between colliding reconnection jets at the center of a magnetic flux rope at the magnetopause. *Geophysical Research Letters*, *43*(11), 5536–5544. https://doi.org/10.1002/2016GL069166

Olsen, N., Lühr, H., Finlay, C. C., Sabaka, T. J., Michaelis, I., Rauberg, J., et al. (2014). The CHAOS-4 geomagnetic field model. *Geophysical Journal International*, *197*, 815–827. https://doi.org/10.1093/gji/ggu033

Panov, E., Büchner, J., Fränz, M., Korth, A., Khotyaintsev, Y., Nikutowski, B., et al. (2006). CLUSTER spacecraft observation of a thin current sheet at the Earth's magnetopause. *Advances in Space Research*, *37*(7), 1363–1372. https://doi.org/10.1029/2006GL026556

Panov, E. V., Artemyev, A. V., Nakamura, R., & Baumjohann, W. (2011). Two types of tangential magnetopause current sheets: Cluster observations and theory. *Journal of Geophysical Research*, *116*(12). https://doi.org/10.1029/2011JA016860

Panov, E. V., Büchner, J., Fränz, M., Korth, A., Savin, S. P., Rème, H., et al. (2008). High-latitude Earth's magnetopause outside the cusp: Cluster observations. *Journal of Geophysical Research*, *113*(A1). https://doi.org/10.1029/2006JA012123

Paschmann, G., & Daly, P. W. (1998). *Analysis methods for multispacecraft data, ISSI science report, SR-001*, (pp. 395–418). Kluwer Academic Pub.

Paschmann, G., & Daly, P. W. (2008). *Multi-spacecraft analysis methods revisited, ISSI science report, SR-008*, (pp. 17–21). Kluwer Academic Pub.

Paschmann, G., Haaland, S., Sonnerup, B. U. Ă., Hasegawa, H., Georgescu, E., Klecker, B., et al. (2005). Characteristics of the near-tail dawn magnetopause and boundary layer. *Annales Geophysicae*, *23*, 1481–1497. https://doi.org/10.5194/angeo-23-1481-2005

Paschmann, G., Haerendel, G., Papamastorakis, I., Sckopke, N., Bame, S. J., Gosling, J. T., et al. (1982). Plasma and magnetic field characteristics of magnetic flux transfer events. *Journal of Geophysical Research*, *87*(A4), 2159. https://doi.org/10.1029/JA087iA04p02159

Paschmann, G., Schwartz, S. J., Escoubet, C. P., & Haaland, S. (2005). Outer magnetospheric boundaries: Cluster results. In G. Paschmann, S. J. Schwartz, C. P. Escoubet, (Eds.) *Reprinted from space science reviews journal* (Vol. 118/1–4, pp. 434). Springer. https://doi.org/10.1007/1-4020-4582-4

Peng, F. Z., Fu, H. S., Cao, J. B., Graham, D. B., Chen, Z. Z., Cao, D., et al. (2017). Quadrupolar pattern of the asymmetric guide-field reconnection. *Journal of Geophysical Research: Space Physics*, *122*(6), 6349–6356. https://doi.org/10.1002/2016ja023666

Perrone, D., Alexandrova, O., Mangeney, A., Maksimovic, M., Lacombe, C., Rakoto, V., et al. (2016). Compressive coherent structures at ion scales in the slow solar wind. *The Astrophysical Journal*, *826*(2), 196. https://doi.org/10.3847/0004-637X/826/2/196

Perrone, D., Alexandrova, O., Roberts, O. W., Lion, S., Lacombe, C., Walsh, A., et al. (2017). Coherent structures at ion scales in fast solar wind: Cluster observations. *The Astrophysical Journal*, *849*(1), 49. https://doi.org/10.3847/1538-4357/aa9022

Petrukovich, A., Artemyev, A., Vasko, I., Nakamura, R., & Zelenyi, L. (2015). Current sheets in the earth magnetotail: Plasma and magnetic field structure with Cluster project observations. *Space Science Reviews*, *188*(1–4), 311–337. https://doi.org/10.1007/s11214-014-0126-7

Phan, T. D., Dunlop, M. W., Paschmann, G., Klecker, B., Bosqued, J. M., Reme, H., et al. (2004). Cluster observations of continuous reconnection at the magnetopause under steady interplanetary magnetic field conditions. *Annales Geophysicae*, *22*(7), 2355–2367. https://doi.org/10.5194/angeo-22-2355-2004

Phan, T. D., Eastwood, J. P., Cassak, P. A., Oieroset, M., Gosling, J. T., Gershman, D. J., et al. (2016). MMS observations of electron-scale filamentary currents in the reconnection exhaust and near the X line. *Geophysical Research Letters*, *43*, 6060–6069. https://doi.org/10.1002/2016GL069212

Pu, Z.-Y., Zhang, X. G., Wang, X. G., Zhou, X.-Z., Xie, L., Dunlop, M. W., et al. (2007). Global view of dayside magnetic reconnection with the dawn-dusk IMF orientation: A statistic study for TC-1 and Cluster data. *Geophysical Research Letters*, *34*, L20101. https://doi.org/10.1029/2007GL030336

Pu, Z. Y., Zong, Q. G., Fritz, T. A., Xiao, C. J., Huang, Z. U., Fu, S. U., et al. (2005). Multiple flux rope events at the high-latitude magnetopause: Cluster/rapid observation on 26 January, 2001. *Surveys in Geophysics*, *26*, 193–214. https://doi.org/10.1007/s10712-005-1878-0

Ritter, P., & Lühr, H. (2013). Determining field-aligned currents with the Swarm constellation mission. *Earth Planets and Space*, *65*, 1285–1294. https://doi.org/10.5047/eps.2013.09.006

Ritter, P., Lühr, H., Viljanen, A., Amm, O., Pulkinnen, A., & Sillanpää, I. (2004). Ionospheric currents estimated simultaneously from CHAMP satellite and IMAGE ground-based magnetic field measurements: A statistical study at auroral latitudes. *Annales Geophysicae*, *22*, 417–430. https://doi.org/10.5194/angeo-22-417-2004

Robert, P., Dunlop, M. W., Roux, A., & Chanteur, G. (1998). Accuracy of current density determination. In *`Analysis methods for multispacecraft data', ISSI science report. SR-001* (pp. 395–418). Kluwer Academic Pub.

Robert, P., Roux, A., Fontaine, D., Canu, P., Le Contel, O., Perraut, S., et al. (2002). Cluster observations of a flux transfer event (FTE). In *COSPAR, Plenary meeting*.

Rong, Z. J., Wan, W. X., Shen, C., Li, X., Dunlop, M. W., Petrukovich, A. A., et al. (2011). Statistical survey on the magnetic structure in magnetotail current sheets. *Journal of Geophysical Research*, *116*, A09218. https://doi.org/10.1029/2011JA016489

Roth, M., De Keyser, J., & Kuznetsova, M. M. (1996). Vlasov theory of the equilibrium structure of tangential discontinuities in space plasmas. *Space Science Reviews*, *76*(3–4), 251–317. https://doi.org/10.1007/BF00197842

Roux, A., Robert, P., Fontaine, D., Le Contel, O., Canu, P., & Louarn, P. (2015). What is the nature of magnetosheath FTEs? *Journal of Geophysical Research: Space Physics*, *120*(6), 4576–4595. https://doi.org/10.1002/2015JA020983

Runov, A., Angelopoulos, V., Sitnov, M. I., Sergeev, V. A., Bonnell, J., McFadden, J. P., et al. (2009). THEMIS observations of an earthward-propagating dipolarization front. *Geophysical Research Letters*, *36*(14), 1–7. https://doi.org/10.1029/2009GL038980

Runov, A., Sergeev, V. A., Baumjohann, W., Nakamura, R., Apatenkov, S., Asano, Y., et al. (2005). Electric current and magnetic field geometry in flapping magnetotail current sheets. *Annales Geophysicae*, *23*, 1391–1403. https://doi.org/10.5194/angeo-23-1391-2005

Runov, A., Sergeev, V. A., Nakamura, R., Baumjohann, W., Apatenkov, S., Asano, Y., et al. (2006). Local structure of the magnetotail current sheet: 2001 Cluster observations. *Annales Geophysicae*, *24*, 247–262. https://doi.org/10.5194/angeo-24-247-2006

Russell, C. T., & Elphic, R. C. (1979). ISEE observations of flux transfer events at the dayside magnetopause. *Geophysical Research Letters*, *6*(1), 33–36. https://doi.org/10.1029/GL006i001p00033

Russell, C. T., Luhmann, J. G., & Strangeway, R. J. (2016). *Space physics: An introduction* (Vol. 978–1107098824). Cambridge University Press. .

Settino, A., Perrone, D., Khotyaintsev, Y., Graham, D., & Valentini, F. (2021). *Kinetic features for the identification of Kelvin-Helmholtz vortices in in-situ observations*. arXiv: 2102.04117.

Shen, C., Dunlop, M., Ma, Y. H., Chen, Z. Q., Yan, G. Q., Liu, Z. X., et al. (2011). The magnetic configuration of the high-latitude cusp and dayside magnetopause under strong magnetic shears. *Journal of Geophysical Research*, *116*, A09228. https://doi.org/10.1029/2011JA016501

Shen, C., & Dunlop, M. W. (2008). Geometric structure analysis of the magnetic field. In G. Paschmann, & P. W. Daly (Eds.), *Multi-spacecraft analysis methods revisited*, Chap. 3. (pp. 27–32): Kluwer Acad.

Shen, C., Li, X., Dunlop, M., Liu, Z. X., Balogh, A., Baker, D. N., et al. (2003). Analyses on the geometrical structure of magnetic field in the current sheet based on cluster measurements. *Journal of Geophysical Research*, *108*(A5), 1168. https://doi.org/10.1029/2002JA009612

Shen, C., Li, X., Dunlop, M., Shi, Q. Q., Liu, Z. X., Lucek, E., et al. (2007). Magnetic field rotation analysis and the applications. *Journal of Geophysical Research*, *112*, A06211. https://doi.org/10.1029/2005JA011584

Shen, C., Liu, Z. X., Li, X., Dunlop, M., Lucek, E., Rong, Z. J., et al. (2008). Flattened current sheet and its evolution in substorms. *Journal of Geophysical Research*, *113*, A07S21. https://doi.org/10.1029/2007JA012812

Shen, C., Rong, J., Dunlop, M., Ma, Y. H., Zeng, G., & Liu, Z. X. (2012). Spatial gradients from irregular, multiple-point spacecraft configurations. *Journal of Geophysical Research*, *117*, A11207. https://doi.org/10.1029/2012JA018075

Shen, C., Rong, Z. J., & Dunlop, M. (2012). Determining the full magnetic field gradient from two spacecraft measurements under special constraints. *Journal of Geophysical Research*, *117*, A10217. https://doi.org/10.1029/2012JA018063

Shen, C., Rong, Z. J., Li, X., Dunlop, M., Liu, Z. X., Malova, H. V., et al. (2008). Magnetic configurations of the tilted current sheets in magnetotail. *Annales Geophysicae*, *26*(11), 3525–3543. https://doi.org/10.5194/angeo-26-3525-2008

Shen, C., Yang, Y. Y., Rong, Z. J., Li, X., Dunlop, M., Carr, C. M., et al. (2014). Direct calculation of the ring current distribution and magnetic structure seen by Cluster during geomagnetic storms. *Journal of Geophysical Research*, *119*, 2458–2465. https://doi.org/10.1002/2013JA019460

Shen, C., Zhang, C., Rong, Z.-J., Pu, Z.-Y., Dunlop, M. W., Escoubet, P., et al. (2021). Non-linear magnetic gradients and complete magnetic geometry from multi-spacecraft measurements. *Journal of Geophysical Research: Space Physics*. https://doi.org/10.1029/2020JA028846

Shen, C., Zhou, Y.-F., Ma, Y.-H., Wang, X.-G., Pu, Z.-Y., & Dunlop, M. W. (2021). A general algorithm for the linear and quadratic gradients of physical quantities based on 10 or more point measurements. *Journal of Geophysical Research: Space Physics*. https://doi.org/10.1029/2021JA029121

Shi, J.-K., Cheng, Z. W., Zhang, T. L., Dunlop, M., & Liu, Z. X. (2009). Properties of field aligned current in plasma sheet boundary layers in magnetotail: Cluster observation. *Chinese Physics Letters*, *26*, 029401. https://doi.org/10.1088/0256-307X/26/2/029401

Shi, J. K., Cheng, Z. W., Zhang, T. L., Dunlop, M., Liu, Z. X., Torkar, K., et al. (2010). South-north asymmetry of field-aligned currents in the magnetotail observed by Cluster. *Journal of Geophysical Research*, *115*. https://doi.org/10.1029/2009JA014446

Shi, J.-K., Guo, J., Dunlop, M., Zhang, T., Liu, Z. X., LucekFazakereleyReme, E. A. H., et al. (2011). Inter-hemispheric asymmetry of the dependence of cusp location on dipole tilt: Cluster observations. *Journal of Geophysical Research*, *30*, 21–26. https://doi.org/10.5194/angeo-30-21-2012

Shi, Q.-Q., Tian, A. M., Bai, S. C., Hasegawa, H., Degeling, A. W., Pu, Z. Y.,et al. (2019). Dimensionality, coordinate system and reference frame for analyzing in-situ space plasma and field data. *Space Science Reviews*. https://doi.org/10.1007/s11214-019-0601-2

Shiokawa, K., Baumjohann, W., Haerndel, G., Paschmann, G., Fennell, J. F., Friis-Christensen, E., et al. (1998). High-speed ion flow, substorm current wedge and multiple Pi2 pulsations. *Journal of Geophysical Research*, *103*(A3), 4491–4507. https://doi.org/10.1029/97JA01680

Shore, R. M., Whaler, K. A., Macmillan, S., Beggan, C., Olsen, N., Spain, T., et al. (2013). Ionospheric midlatitude electric current density inferred from multiple magnetic satellites. *Journal of Geophysical Research: Space Physics*, *118*, 5813–5829. https://doi.org/10.1002/jgra.50491

Sibeck, D. G., Lopez, R. E., & Roelof, E. C. (1991). Solar wind control of the magnetopause shape, location, and motion. *Journal of Geophysical Research*, *96*(A4), 5489–5495. https://doi.org/10.1029/90JA02464

Slavin, J. A., Lepping, R. P., Gjerloev, J., Goldstein, M. L., Fairfield, D. H., Acuna, M. H., et al. (2003). Cluster electric current density measurements within a magnetic flux rope in the plasma sheet. *Geophysical Research Letters*, *30*, 1362. https://doi.org/10.1029/2002GL016411

Stawarz, J. E., Matteini, L., Parashar, T. N., Franci, L., Eastwood, J. P., Gonzalez, C. A., et al. (2021). Comparative analysis of the various generalized Ohm's law terms in magnetosheath turbulence as observed by Magnetospheric Multiscale. *Journal of Geophysical Research: Space Physics*, *126*, e2020JA028447. https://doi.org/10.1029/2020ja028447

Sun, W. J., Fu, S. Y., Parks, G. K., Liu, J., Yao, Z. H., Shi, Q. Q., et al. (2013). Field-aligned currents associated with dipolarization fronts. *Geophysical Research Letters*, *40*(17), 4503–4508. https://doi.org/10.1002/grl.50902

Takada, T., Nakamura, R., Baumjohann, W., Seki, K., Voros, Z., Asano, Y., et al. (2006). Alfven waves in the near-psbl lobe: Cluster observations. *Annales Geophysicae*, *24*, 1001–1013. https://doi.org/10.5194/angeo-24-1001-2006

Tang, B. B., Wang, C., & Guo, X. C. (2012). Bow shock and magnetopause contributions to the magnetospheric current system: Hints from the Cluster observations. *Journal of Geophysical Research: Space Physics*, *117*(1). https://doi.org/10.1029/2011JA016681

Teh, W. L., Nakamura, T. K. M., Nakamura, R., Baumjohann, W., Russell, C. T., Pollock, C., et al. (2017). Evolution of a typical ion-scale magnetic flux rope caused by thermal pressure enhancement. *Journal of Geophysical Research: Space Physics*, *122*(2), 2040–2050. https://doi.org/10.1002/2016JA023777

Thompson, S. M., Kivelson, M. G., El Alaoui, M., Balogh, A., Reme, H., & Kistler, L. M. (2006). Bifurcated current sheets: Statistics from cluster magnetometer measurements. *Journal of Geophysical Research*, *111*, A03212. https://doi.org/10.1029/2005JA011009

Thompson, S. M., Kivelson, M. G., Khurana, K. K., Balogh, A., Réme, H., Fazakerley, A. N., et al. (2004). Cluster observations of quasi-periodic impulsive signatures in the dayside northern lobe: High-latitude flux transfer events? *Journal of Geophysical Research: Space Physics*, *109*(A2). https://doi.org/10.1029/2003JA010138

Torbert, R. B., Burch, J. L., Giles, B. L., Gershman, D., Pollock, C. J., Dorelli, J., et al. (2016). Estimates of terms in Ohm's law during an encounter with an electron diffusion region. *Geophysical Research Letters*, *43*(12), 5918–5925. https://doi.org/10.1002/2016GL069553

Torbert, R. B., Burch, J. L., Phan, T. D., Hesse, M., Argall, M. R., Shuster, J., et al. (2018). Electron-scale dynamics of the diffusion region during symmetric magnetic reconnection in space. *Science*. https://doi.org/10.1126/science.aat2998

Trenchi, L., The FAC-MICE Team, Kauristie, K., Käki, S., Vanhamäki, H., Juusola, L., et al. (2020). ESA field-aligned currents – Methodology inter-comparison exercise. In M. W. Dunlop, & H. Luehr (Eds.), *Ionospheric multi-satellite analysis tools, ionosphere. ISSI scientific reports* (Vol. 17). Springer. https://doi.org/10.1007/978-3-030-26732-2_8

Vallat, C., Dandouras, I., Dunlop, M., Balogh, A., Lucek, E., Parks, G. K., et al. (2005). First current density measurements in the ring current region using simultaneous multi-spacecraft CLUSTER-FGM data. *Annales Geophysicae*, *23*, 1849–1865. https://doi.org/10.5194/angeo-23-1849-2005

Vogt, J., Albert, A., & Marghitu, O. (2009). Analysis of three-spacecraft data using planar reciprocal vectors: Methodological framework and spatial gradient estimation. *Annales Geophysicae*, *27*, 3249–3273. https://doi.org/10.5194/angeo-27-3249-2009

Vogt, J., Paschmann, G., & Chanteur, G. (2008). Reciprocal vectors. In G. Paschmann, & P. W. Daly (Eds.), *`Multi-Spacecraft analysis methods revisited. ISSI science report, SR-008* (pp. 27–30). Kluwer Academic Pub.

Vogt, J., Sorbalo, E., He, M., & Blagau, A. (2013). Gradient estimation using configurations of two or three spacecraft. *Annales Geophysicae*, *31*, 1913–1927. https://doi.org/10.5194/angeo-31-1913-2013

Volwerk, M., Glassmeier, K. H., Runov, A., Baumjohann, W., Nakamura, R., Zhang, T. L., et al. (2003). Kink mode oscillation of the current sheet. *Geophysical Research Letters*, *30*, 1320. https://doi.org/10.1029/2002GL016467

Vörös, Z., Yordanova, E., Varsani, A., Genestreti, K. J., Khotyaintsev, Y. V., Li, W., et al. (2017). MMS observation of magnetic reconnection in the turbulent magnetosheath. *Journal of Geophysical Research: Space Physics*, *122*(11), 11–442. https://doi.org/10.1002/2017ja024535

Wang, H., Ma, S. Y., Lühr, H., Liu, Z. X., Pu, Z. Y., Escoubet, C. P., et al. (2006). Global manifestations of a substorm onset observed by a multi-satellite and ground station network. *Annales Geophysicae*, *24*, 3491–3496. https://doi.org/10.5194/angeo-24-3491-2006

Wang, R., Lu, Q., Nakamura, R., Baumjohann, W., Russell, C. T., Burch, J. L., et al. (2017). Interaction of magnetic flux ropes via magnetic reconnection observed at the magnetopause. *Journal of Geophysical Research: Space Physics*, *122*(10), 10–436. https://doi.org/10.1002/2017ja024482

Wang, T., Alexandrova, O., Perrone, D., Dunlop, M., Dong, X., Bingham, R., et al. (2019). Magnetospheric multiscale observation of kinetic signatures in the Alfvén vortex. *The Astrophysical Journal Letters*, *871*(2), L22. https://doi.org/10.3847/2041-8213/aafe0d

Wendel, D. E., & Adrian, M. L. (2013). Current structure and nonideal behavior at magnetic null points in the turbulent magnetosheath. *Journal of Geophysical Research: Space Physics*, *118*(4), 1571–1588. https://doi.org/10.1002/jgra.50234

Xiao, C., Liu, W., Shen, C., Zhang, H., & Rong, Z. (2018). Study on the curvature and gradient of the magnetic field in Earth's cusp region based on the magnetic curvature analysis method. *Journal of Geophysical Research: Space Physics*, *123*. https://doi.org/10.1029/2017ja025028

Xiao, C. J., Pu, Z. Y., Ma, Z. W., Fu, S. Y., Huang, Z. Y., & Zong, Q.-G. (2004). Inferring of flux rope orientation with the minimum variance analysis technique. *Journal of Geophysical Research*, *109*, A11218. https://doi.org/10.1029/2004JA010594

Xiao, C. J., Wang, X. G., Pu, Z. Y., Zhao, H., Wang, J. X., Ma, Z. W., et al. (2006). In situ evidence for the structure of the magnetic null in a 3D reconnection event in the Earth's magnetotail. *Nature Physics*, *2*, 478–483. https://doi.org/10.1038/nphys342

Yang, Y.-Y., Shen, C., Dunlop, M., Rong, Z.-J., Li, X., Angelopolous, V., et al. (2016). Storm time current distribution in the inner magnetospheric equator: THEMIS observations. *Journal of Geophysical Research: Space Physics*, *120*. https://doi.org/10.1002/2015JA022145

Yang, Y. Y., Shen, C., Zhang, Y. C., Rong, Z. J., Li, X., Dunlop, M., et al. (2014). The force-free configuration of flux ropes in geomagnetotail: Cluster observations. *Journal of Geophysical Research: Space Physics*, *119*, 6327–6341. https://doi.org/10.1002/2013JA019642

Yao, S. T., Shi, Q. Q., Guo, R. L., Yao, Z. H., Fu, H. S., Degeling, A. W., et al. (2020). Kinetic-scale flux rope in the Magnetosheath boundary layer. *The Astrophysical Journal*, *897*(2), 137. https://doi.org/10.3847/1538-4357/ab9620

Yao, Z., Sun, W. J., Fu, S. Y., Pu, Z. Y., Liu, J., Angelopoulos, V., et al. (2013). Current structures associated with dipolarization fronts. *Journal of Geophysical Research: Space Physics*, *118*(11), 6980–6985. https://doi.org/10.1002/2013JA019290

Yao, Z. H, Pu, Z. Y., Owen, C. J., Fu, S. Y., Chu, X. N., Liu, J., et al. (2014). Current reduction in a pseudo-breakup event: THEMIS observations. *Journal of Geophysical Research: Space Physics*, *119*(10), 8178–8187. https://doi.org/10.1002/2014JA020186

Yordanova, E., Vörös, Z., Varsani, A., Graham, D. B., Norgren, C., Khotyaintsev, Y. V., et al. (2016). Electron scale structures and magnetic reconnection signatures in the turbulent magnetosheath. *Geophysical Research Letters*, *43*(12), 5969–5978. https://doi.org/10.1002/2016GL069191

Zenitani, S., Hesse, M., Klimas, A., & Kuznetsova, M. (2011). New measure of the dissipation region in collisionless magnetic reconnection. *Physical Review Letters*, *106*, 195003. https://doi.org/10.1103/PhysRevLett.106.195003

Zhang, L. Q., Baumjohann, W., Dai, L., Khotyaintsev, Y. V., & Wang, C. (2019). Measurements of the vorticity in the bursty bulk flows. *Geophysical Research Letters*, *46*. https://doi.org/10.1029/2019gl084597

Zhang, L. Q., Lui, A. T. Y., Baumjohann, W., Wang, C., Burch, J. L., & Khotyaintsev, Y. V. (2020). Anisotropic vorticity within bursty bulk flow turbulence. *Journal of Geophysical Research: Space Physics*, *125*, e2020JA028255. https://doi.org/10.1029/2020JA028255

Zhang, Q.-H., Dunlop, M. W., Lockwood, M., Holme, R., Kamide, Y., Baumjohann, W., et al. (2011). The distribution of the ring current: Cluster observations. *Annales Geophysicae*, *29*, 1655–1662. https://doi.org/10.5194/angeo-29-1655-2011

Zhang, T. L., Baumjohann, W., Nakamura, R., Runov, A., Volwerk, M., Asano, Y., et al. (2006). A statistical survey of the magnetotail current sheet. *Advances in Space Research*, *38*, 1834–1837. https://doi.org/10.1016/j.asr.2006.05.009

Zhang, Y. C., Shen, C., Liu, Z., & Rong, Z. J. (2013). Two different types of plasmoids in the plasma sheet: Cluster multisatellite analysis application. *Journal of Geophysical Research: Space Physics*, *118*, 5437–5444. https://doi.org/10.1002/jgra.50542

Zhang, Y. C., Shen, C., Marchaudon, A., & Rong, Z. J. (2016). First in situ evidence of electron pitch angle scattering due to magnetic field line curvature in the Ion diffusion region. *Journal of Geophysical Research: Space Physics*, *121*. https://doi.org/10.1002/2016JA022409

Zhao, C., Russell, C. T., Strangeway, R. J., Petrinec, S. M., Paterson, W. R., Zhou, M., et al. (2016). Force balance at the magnetopause determined with MMS: Application to flux transfer events. *Geophysical Research Letters*, *43*(2311), 941947–942011. https://doi.org/10.1002/2016GL071568

Zhong, Z. H., Deng, X. H., Zhou, M., Ma, W. Q., Tang, R. X., Khotyaintsev, Y. V., et al. (2019). Energy conversion and dissipation at dipolarization fronts: A statistical overview. *Geophysical Research Letters*, *46*, 12693–12701. https://doi.org/10.1029/2019gl085409

Zhou, M., Ashour-Abdalla, M., Berchem, J., Walker, R. J., Liang, H., El-Alaoui, M., et al. (2016). Observation of high-frequency electrostatic waves in the vicinity of the reconnection ion diffusion region by the spacecraft of the Magnetospheric Multiscale (MMS) mission. *Geophysical Research Letters*, *43*(10), 4808–4815. https://doi.org/10.1002/2016gl069010

Zhou, M., Deng, X. H., Li, S. Y., Pang, Y., Vaivads, A., Rème, H., et al. (2009). Observation of waves near lower hybrid frequency in the reconnection region with thin current sheet. *Journal of Geophysical Research*, *114*(A2). https://doi.org/10.1029/2008JA013427

Zhou, M., Pang, Y., Deng, X. H., Yuan, Z. G., & Huang, S. Y. (2011). Density cavity in magnetic reconnection diffusion region in the presence of guide field. *Journal of Geophysical Research*, *116*(A6). https://doi.org/10.1029/2010JA016324

Zuo, P. B., Liu, S. L., Jin, S. P., Liu, Z. X., & Shi, J. K. (2004). A study of the characteristics for the magnetic flux transfer events occurred on March 2, 2001. *Chinese Journal of Geophysics-Chinese Edition*, *47*(3), 376–384. https://doi.org/10.1002/cjg2.503